AD_____

Award Number: W81XWH-07-2-0085

TITLE: Improving Soldier Recovery from Catastrophic Bone Injuries: Developing an Animal Model for Standardizing the Bone Reparative Potential of Emerging Progenitor Cell Therapies

PRINCIPAL INVESTIGATOR: Dr. David Rowe, M.D.

CONTRACTING ORGANIZATION: University of Connecticut
Farmington, CT 06032

REPORT DATE: August 2011

TYPE OF REPORT: Final

PREPARED FOR: U.S. Army Medical Research and Materiel Command
Fort Detrick, Maryland 21702-5012

REPORT DOCUMENTATION PAGE

Form Approved
OMB No. 0704-0188

1. REPORT DATE *(DD-MM-YYYY)*	2. REPORT TYPE	3. DATES COVERED *(From - To)*
01-08-2011	Final	1 AUG 2007 - 31 JUL 2011

4. TITLE AND SUBTITLE
Improving Soldier Recovery from Catastrophic Bone Injuries: Developing an Animal Model for Standardizing the Bone Reparative Potential of Emerging Progenitor Cell Therapies

5a. CONTRACT NUMBER

5b. GRANT NUMBER
W81XWH-07-2-0085

5c. PROGRAM ELEMENT NUMBER

6. AUTHOR(S)
Dr. David Rowe, M.D.

E-Mail: rowe@neuron.uchc.edu

5d. PROJECT NUMBER

5e. TASK NUMBER

5f. WORK UNIT NUMBER

7. PERFORMING ORGANIZATION NAME(S) AND ADDRESS(ES)
University of Connecticut
Farmington, CT 06032

8. PERFORMING ORGANIZATION REPORT NUMBER

9. SPONSORING / MONITORING AGENCY NAME(S) AND ADDRESS(ES)
U.S. Army Medical Research and Materiel Command
Fort Detrick, Maryland 21702-5012

10. SPONSOR/MONITOR'S ACRONYM(S)

11. SPONSOR/MONITOR'S REPORT NUMBER(S)

12. DISTRIBUTION / AVAILABILITY STATEMENT
Approved for Public Release; Distribution Unlimited

13. SUPPLEMENTARY NOTES

14. ABSTRACT

During the final year of this award, we have completed the analysis of three different models of skeletal repair that can be used to assess different strategies of progenitor cells, scaffolds and host preparation used to heal a critical sized defect. GFP reporters harbored in the mice provide a cellular explanation for the outcome and image analytical techniques afford an objective quantitation of the results. The major finding include: (1) the importance of the right type of progenitor cells for type of skeletal defect to be repaired; (2) the importance of robust progenitor cells which are easily obtained from the mice but will be a challenge for human donor sources; (3) the subtle but highly structured cellular response to fracture repair and its relevance to successful healing of a segmental long bone defect. Multipotential progenitors, marked by a SMAA reporter recreate the bone, cartilage and periosteum and each structure plays a necessary role in a successful repair; discovery that a sublineage distinct from osteoblasts and marked by a DKK3 reporter leads to fibrocartilage and periosteal development; (4) the cryohistology that facilitates the rapid and informative analysis of a repair defect can be applied to non-transgenic models including larger animals; (5) a concept of centralized and uniform processing and imaging of repair defects accessible via database archiving is present that would be useful in identifying the most promising repair strategies and providing the most consistent preclinical data for approval for clinical trials.

15. SUBJECT TERMS
No subject terms provided.

16. SECURITY CLASSIFICATION OF:			17. LIMITATION OF ABSTRACT	18. NUMBER OF PAGES	19a. NAME OF RESPONSIBLE PERSON
a. REPORT	b. ABSTRACT	c. THIS PAGE			USAMRMC
U	U	U	UU	39	19b. TELEPHONE NUMBER *(include area code)*

Standard Form 298 (Rev. 8-98)
Prescribed by ANSI Std. Z39.18

Table of Contents

Page

Introduction **4**

Body **5**

Objective 1: Calvarial transplantation model **5**

A. Knowledge gained over the life of the grant. 5

B. Progress over the past year 6

C. Implications for future research 10

Objective 2A: Establish the long bone fracture/repair model **12**

A. Knowledge gained over the life of the grant. 12

B. Progress over the past year including the 1 year extension: the Dkk3 lineage. 14

C. Implications for future research 17

Objective 2B: Gain experience with the long bone segmental defect **17**

A. Knowledge gained over the life of the grant 17

B. Progress over the past year 18

C. Implications for future research 20

Objective 3A: Image analysis of repair lesions **21**

A. Knowledge gained over the life of the grant 21

B. Progress over the past year 22

C. Implications for future research 24

Objective 3B: Archiving and retrieving histological images **25**

A. Knowledge gained over the life of the grant 25

B. Progress over the past year 25

C. Implications for future research 26

KEY RESEARCH ACCOMPLISHMENTS **26**

REPORTABLE OUTCOMES FOR YEAR 3-4 ..... **27**

Conclusion **29**

INTRODUCTION

This proposal was developed to face the reality that the most optimal scaffold, cell source and host preparation for repair of a critical sized skeletal defect is yet to defined. Furthermore the best combination of these factors is likely to be identified in a trial and error approach. This is unlikely to be hypothesis driven research nor is it a process that can be adequately explored in traditional large animal models. We want to demonstrate that a fast, informative, quantitative and biologically relevant process to initially screen for the most promising candidate factors can be developed using a series of GFP-reporter mice and bone repair models. The 2010-updated reporters most frequently referred to in the experimental descriptions and their position within the osteoblast lineage are given in figure 1. As the best tissue engineering strategies are identified,

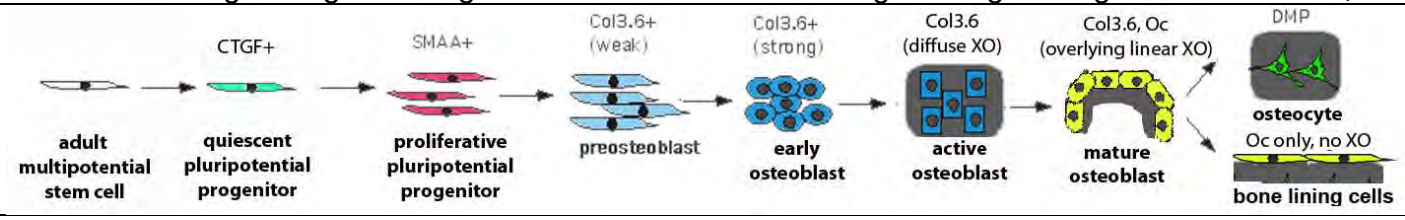

Figure 1: Association of GFP reporters with levels of osteoprogenitor differentiation. When all three transgenes are in the same mouse, the color overlap (SMAAred/Col3.6blue and Col3.6/Ocgreen) at intermediate levels of progression. New to the lineage is CTGF+ cells that appear to identify quiescent trabecular bone lining progenitor cells. A mouse expressing telomerase (mtert) has been recently acquired and will be evaluated as another quiescent progenitor cell.

they will be evaluated in an increasingly more demanding repair setting so that at the end of the process a rational process can select the protocols most deserving of evaluation in a large animal model. We have worked on our longer-range goal to adapt the models and reporter systems to: 1) larger non-GFP based animal repair models (rat and rabbit) and 2) murine models capable of evaluating human derived progenitor cells as the basis for eventual clinical trials. Our year 3 statement of work (SOM) as presented in the application is directed at extending the models of repair with a particular focus on the segmental long bone defect.

- *Utilize the best source of osteoprogenitor cells to characterize the cellular activities (host and donor) that participate in our two models of skeletal repair. New reporters (CTGF, TRAP) have been introduced that further refine the lineages that are activated in repair. New fluorescence based staining protocols (AP and TRAP) have been implemented to associate molecular activity with cellular sources in models that lack GFP, particularly when the donor source is human. We have begun an investigation to determine if low oxygen conditions promoter the expansion of osteoprogenitor cells that retain their bone differentiation properties.*
- *Work closely with material scientists (Wei and Nair) who have produced various scaffolds for introducing progenitor cells into the calvarial defect model to determine modifications that will enhance the osteogenic properties of the scaffold.*
- *Increase the through put, objectivity and recall of data that is generated from these images using a new acquired automated microscope system (Mirax Midi), in house developed image analysis algorithms for bone cell dynamics and databases for storage and retrieval of data.*

It was a very sobering third year as we truly began to appreciate the challenges that need to be overcome before cell based therapy will even be properly understood or evaluated in human subjects. It is clear the FDA will be requiring very convincing preclinical data before any progenitor cells studies will be permitted. This report is organized to summarize what has been learned during the 3 year grant period and the new information gained in the final year. Each section also discusses the implication of these results to future research toward an eventual human application.

BODY

Objective 1: Calvarial transplantation model

The calvarial defect has continued to be a robst and informative platform to evaluate progenitor and scaffold combination. The most reliable and rapid protocol deposits test progenitor cells directly into a 1.5 mm thick Healos disc after the scaffold has been implanted into the defect. Depending on the experimental question, either a single to a double hole format can be employed. We have come to appreciate that this model has the highest through put for initial screening of the osteogenic potential of a cell population. In contrast to the widely used heterotopic assay, the ability of the donor cells to form a recognized bone structure and to integrate with host bone can be evaluated. Even X-ray, μCT and Ivis evaluations are easier to interpret and relate to the subsequent histology. Technically the model has proven to be exceptionally valuable for initial evaluation of progenitors, host factors and scaffolds.

A. Knowledge gained over the life of the grant.

1. *mCOB is the most convenient and reliable source of osteoprogentors* – Neonatal (day 4-7) calvaria enzymatic digest cells, whether used directly or expanded for 4-5 days in primary culture consistently differentiate into a serpentine membraneous bone structure with relatively few marrow elements. However it show little propensity to integrate with host bone and in fact when placed in a segmental defects, they are inhibitory to the periosteal response characteristic of a bone fracture. Because our primary long term interest is repair of segmental defects, we rarely use this source of progenitors. Furthermore they are not a clinically revelant source of progentors.

2. *Fresh bone marrow lacks inherent progenitor activity*. Despite its wide clinical use, marrow cleared of bone fragments has no bone forming activity in the calvarial defect whether administered alone or in combination with mCOB. Reporter studies do indicate that the marrow contributes to a cell population that lines the bone surface, but these cells do not deposit mineral and they carry markers of osteoclasts or osteomacs. Similarly designed experiments demonstrate bone marrow derived cells (either from the host or a parabion) can be shown to explain the erroneour claim of circulating osteoprogenitor cells.

3. *Bone marrow gains its progenitor potential after 3-5 days in primary culture*. Upon initiating a BMSC culture, a subpopulation of cells that attach begin to proliferate to form loose clusters of cells. These cells are both express the SMAA and CTGF reporter activity, and microarray analysis shows expression of genes consistent with the osteogenic lineage. Transplantation of the sorted cells cells will generate bone carrying markers of the donor. In our standard transplantation assay, a heterogeneous mixture of plastic adherent cells is implanted into the healos scaffold and results in a structure that resembles cortical bone with a highly enrighed bone marrow component. In contrast, when the non-adherent cells are implanted, no bone is formed in contrast to what is claimed by others (these cells are primarily marrow elements and give rise to bone surface associated osteoclasts and osteomacs.) The adherent BMSCs have become our primary source of progenitors for most experiments. The primary drawback is the relatively small numbers of cells that can be harvested from donor animals. This problem is being addressed (see future directions).

4. *Cortical bone outgrowth cells have progenitor potential* – Another clinically relevant source are the cells that can be grown out from bone chips. These cells undergo one round of passage after their intial 8-10 day initial outgrowth to produce a relatively large number of progenitors approximately two weeks after the initial harvest. The cells express the SMAA reporter and molecular markers of bone progenitor cells. The bone produced is cortical but it is not as well developed as the primary BMSC cultured cells. We are not pursuing this source and suspect that the prolonged culture is compromising progenitor potential (see future directions.)

5. *Adipose stromal cells (AdSC) lack osteoprogenitor activity* – AdSC form a cellular layer that is almost exclusively SMAA positive but it does not express markers of early osteogenesis as found in the BMSC and chip outgrowth cells. When implanted into a calvarial defect, no bone is formed. We have not evaluated AdSC treated in vitro with BMPs, as is ususally done to achieve osteogenesis, because our goal is to identify progenitors with inherent osteogenic activity.

A manuscript describing the properties of the calvarial defect model is in preparation.

B. Progress over the past year

1. Use of Calvarial defect model for scaffold testing

a. Collaboration with Dr. Mei Wei - We have continue our interaction with Dr. Wei and her graduate student (Mr. Xiaohua Yu) that began as an NIH funded sabbatical. Dr. Mei Wei from the Department of Material Sciences/School of Engineering at UCONN Storrs. After making multiple modification to her scaffold prepartion (see last year's report), they were able to formulate a collagen/HA structure that performed as well as commercially prepared Healos. This experience taught both of us that theoretical properties of a scaffold are not necessarily immediately realized in vivo. Multiple failures in the low cost murine model eventually did result in a biocompatible formulation. In addition it taught a PI and graduate student volumes about histology and histological interpretation, a subject that is not highly stressed in the material science world.

During the current year they pursued an preliminary observation that a laminated form of the collagen/HA scaffold rather a random structure resembling Healos led to more robust and consistent osteogenic differentiation of the calvarial progenitor than the network design. When BMSC were used to compare the two formulation, bone formed earlier in the laminated structure. Eventually, equivalent amounts of bone were produce with the laminated structure leading to better host integration of the newly formed bone. The other difference of the formulation (laminate or random) was a more trabeculated structure that the cortical bone structure seen with the Healos material. A manuscript of this work will be submitted shortly.

b. Collaboration with Dr. Lakshmi Nair – With the establishment of Dr. Cato Laurencin's group in adjacent laboratory space to ours, we have begun to explore how our surgical models can be integrated with their material science efforts. Most productive to date has be experiments with Dr. Lakshmi Nair utilizing chitosan and lactoferrin based carriers induced to form a soft gel within the defect area. Again, gellation in vitro did not correlate well with in vivo, so a number of modification to the liquid carrier was required before the cell were retained within the defect space. This effort has progressed to the point that she was successful in securing a DOD award, "Inductive Microenvironment for Improved Osseous Integration: Developing an Animal Model for Standardizing the Bone Reparative Potential of Emerging (Proposal Number OR090591) utilizing our reporter mice and histology. In addition, the resubmission of our 2010 ear mark proposal has one project with Dr. Yusuf Kahn from the Laurencin group examining various designs of PLAGA microbeads with secondary phase hydrogel or nanofiber mesh structures as a weight bearing scaffold for skeletal repair. This biocompatibility of this design will be first evaluated in the calvarial defect before migrating to a segmental defect in mouse or rat.

c. In vitro matrix testing – During the final year of this grant, Drs. Kuhn and Goldberg direct the majority of their attention to the hES derived progenitor cells as described below. They completed their work with the in vitro evaluation of osteogenesis on scaffolds surfaces resulting in the publication (see publication #5)

Thus the calvarial defect model, using proven progenitor cells, is an appropriate model first to evaluate the biocompatibility (biologic and physical) with a non-loaded skeletal defect and second, to determine if it is conducive for the progenitor cells to differentiate to osteoblast and to recruit osteoclasts and macrophages to resorb the scaffold. The experience has also been helpful in developing a way to coordinate multiple participants generating differents type of experimental results and to associate all this information with the resulting histology (see later…).

2. Use of calvarial model to assess bone progenitor activity of human cells – Utilizing funds from our State Stem Cell grant, we have used the calvarial defect model in mice derived from our nod/scid/common gamma chain KO mouse colony (NSG) which is the best immunocompomised mouse line for long term human cell engraftment. That grant ended in 4/10 and we continue the work with this DOD grant because by then we were anticipating that the renewal would focus on human derived progenitors. All of this work uses IRB and ESCRO approved protocols and NIH approved hES cell lines (H9).

a. BMSC derive progenitor cells – Based on the claims for osteogenesis made by commercial companies such as Lonza and ScienCell Research Labs, we began by acquiring one of these products (Lonza) and testing their bone forming activity in the calvarial system. This was

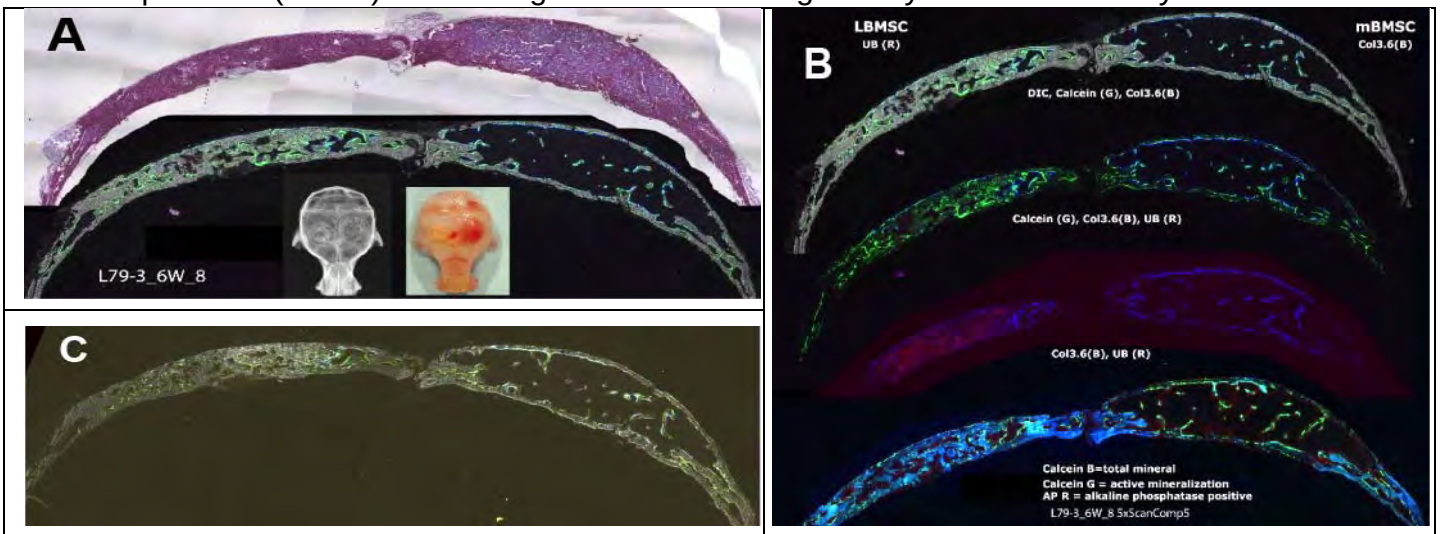

Figure 2: Calvarial defect implanted with hBMSC (Lonza, ubiquitin-RFPcherry) on the left and mBMSC (Col3.6blue) on the right. A. H&E and DIC/fluorescence scan along with Xray and photograph show the typical cortical like bone made by the mBMSC and a dense, partially mineralized structure (green=calcein labeling) on the left. B. Individual fluorescent channels with the DIC removed. Green is areas of active mineralization while blue is a post-section calcein blue stain that shows areas of mineral accumulation. Note that there is a diffuse red signal coming from the left side indicating the presence of the hBMSC-derived cells carrying the ubiquitin-red reporter. However Col3.6blue cells are also present on the medial side, indicating crossover from the right side. C. ELF97 stain for alkaline phosphatase activity, which is strongest in the same area as the strong calcein green staining on hBMSC side of the defect.

a low passage line that was transduced with a lentiviral vector expressing a ubquitin-RFPcherry reporter during its initial passaging step prior to implantation. We estimated that approximately 25% of the population was carrying the reporter at the time of transplant. As a control, mouse BMSC carrying the Col3.6blue reporter was loaded into the contralateral defect (right side, figure 2A). As expected the mBMSC made a cortical bone structure with ample marrow investment, which is obvious even from the photograph of the dissected calvaria. However the mineralized material that forms on the right side is complex and not easily explained. Host bone appears to have grown inward from the lateral margin but this area also has unresorbed hydrolyapatite from the Healos. Medially active bone formation is evident and it has a more membraneous character despite the contribution from the mBMSC that contaminated the area. Figure 2B which has the DIC turned off, better illustrates the bone forming activity by calcein labeling (green) and the red and blue cellular activity. The lower image of figure 2B is a calcein blue stain which identifies total mineral accumulation. Figure 2C is an Elf97 stain for alkaline phosphatase (AP) showing the most of the bone forming activity is associated with the Col3.6 cells and not the region which has the red signal from the ubiq-RFP donor cells.

Figure 3 is a higher power view of the bone forming region of the right defect showing that in areas where bone labeling is observed, Col3.6blue is evident over the calcein label along with randomly scattered Ubiq-RFP human cells. With the DIC turned off, the calcein label shows that Col3.6 blue and non-GFP marked cells predominate with few of the red cells in a similar location.

Figure 2C Co-localization for AP show strong activity over areas of Col3.6blue cells but no activity over the red cells. Not show but illustrated below, an immunostain for human cells was localized to the numerous cells within the transplanted tissue, but these cells were not over a calcein label. Our interpretation is that bone did form within in the repair tissue, but the bone formed was either host or mBMSC in origin. The human cells did not contribute significantly to the disorganized bone that was formed in the region.

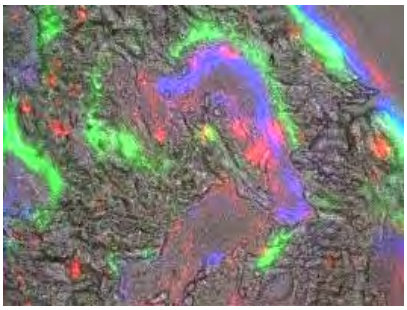

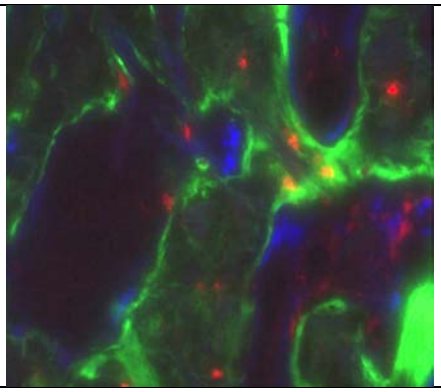

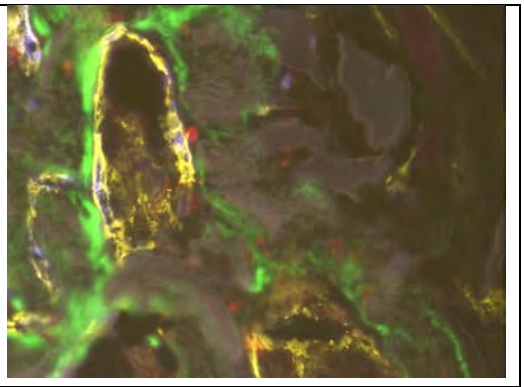

Figure 3: High power images through the area of active bone formation of figure x. A. DIC showing the mineralized tissue containing green calcein mineralization lines with Col3.6blue and human Ubiq-red cells. The red cells are randomly distributed while the blue are localized over the mineralization lines. B. With the DIC removed, the cells in association with the calcein labeling lines are better appreciated. Many of the green lines lack a fluorescent label indicating that they probably arose from the host (non-transgenic NSG mouse). C. ELF97 yellow fluorescent stain for AP activity that strongly coats the surface of the Col3.6blue cells. No staining of ubiq-red cells was observed.

The same cells that were implanted into the mice were also used to initiate cultures for in vitro osteogenesis. Traditional osteogenic conditions (ascorbic acid, dexamethasone, ß-glycerol phosphate failed to initiate mineralizing colonies similar to those seen in murine cultures. Only the addition of BMP4 induced formation of regions resembling clusters of osteogenic cells. Recently we established a BMSC culture from a primary bone marrow explant and the second passage of these cell did spontaneously form bone nodules. Currently these cells are being tested in the calvarial model. We suspect that the osteogenic potential of the commercial hBMSC, like murine cells, is rapidly lost with continued passage under traditional cell culture conditions.

b. hES derived progenitor cells – The primary objective of our Connecticut Stem Cell grant was to direct either hES or iPS cells into the osteogenic lineage. Our frustration during that project was that none of the published or suggested protocols resulted in any evidence of convincing osteogenesis either in primary culture or by calvarial transplant. However Dr. Liisa Kuhn appeared to have success using a prolonged culture using an epithelial differentiation protocol in which the cells are induce to form an flattened morphology. Upon replacement of the medium with a mesenchymal culture condition, the cells become more fibroblastic in morphology and are claimed to be osteogenic. There is some embryonic rational for an epithelial->mesenchymal transition during the initial germ layer formation. While these cells did not form osteogenic nodules in vitro, they did generate significant bone upon transplantation into NSG mice.

Figure 4 illustrates the low power view across both defects which each received the E->M differented cells. Cells that filled the right defect has also been transduced with a lentiviral vector expressing a Col2.3eGFP reporter. Two distinct regions have developd in each repair field. A deep layer of newly formed membraneous bone with active mineralization lines has develop as an extension of the host bone. Above this region is a loose network of cells resembling the blastema of a repairing digit that are stained blue with DAPI. Initially were encouraged that some of the implanted hES cells may have differentiated into osteoblasts because a cells expressing the Col2.3eGFP reporter appeared to overlie a red mineralization label. However further testing indicate these cells do not show staining for AP but instead appear to lie between the AP positive

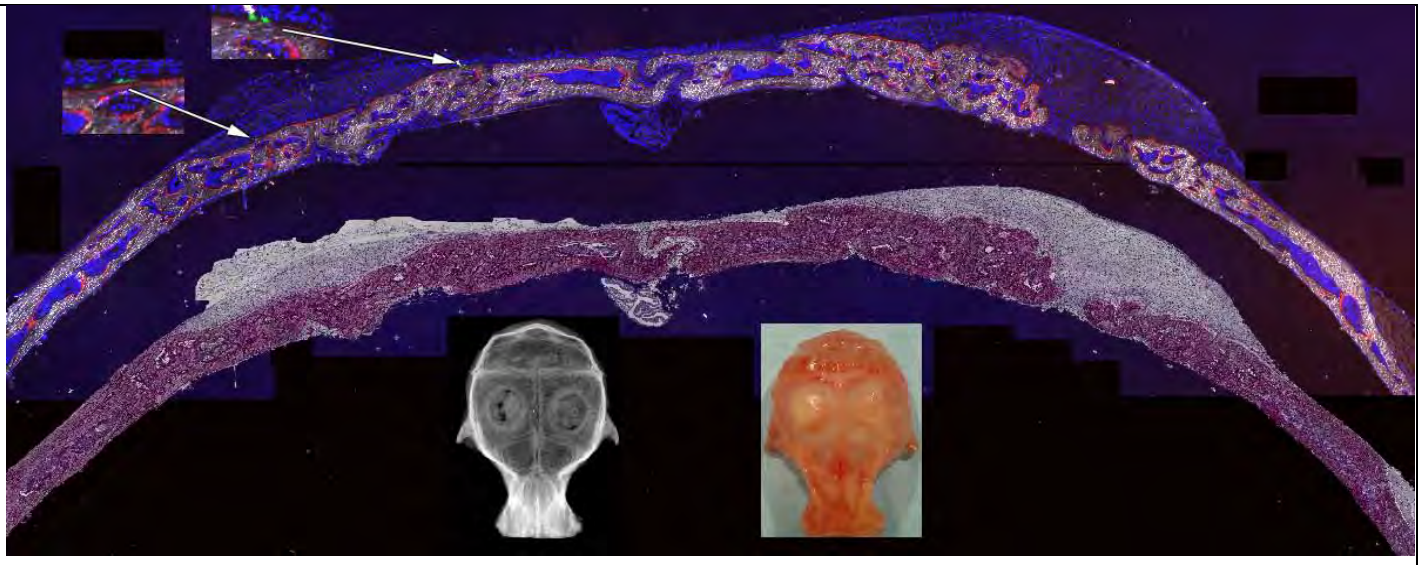

Figure 4: Osteogenesis in the NSG mice from hES derived progenitor cells. The full calvarial view has the DAPI stained (blue) fluorescence on top that was subsequently stained with hematoxylin. The right hole was filled with progenitors that had been transduced with a Col2.3GFP lentiviral vector and the arrows point to a few cells that have the characteristic expression of ostogenic Col2.3GFP (bright green over a red alizarin red complexone labeling line).

osteoblastic cells (presumably unlabeled host) and the underlying red mineralization line (see figure 5). Thus we cannot conclude that the human cells carrying the Col2.3 reporter are osteoblastic cells. The study underlies the importance of having a GFP reporter to mark host derived cells to help distinguish the source of the bone forming activity. These mice are being generated (see objective 3A) but will not be available for another year.

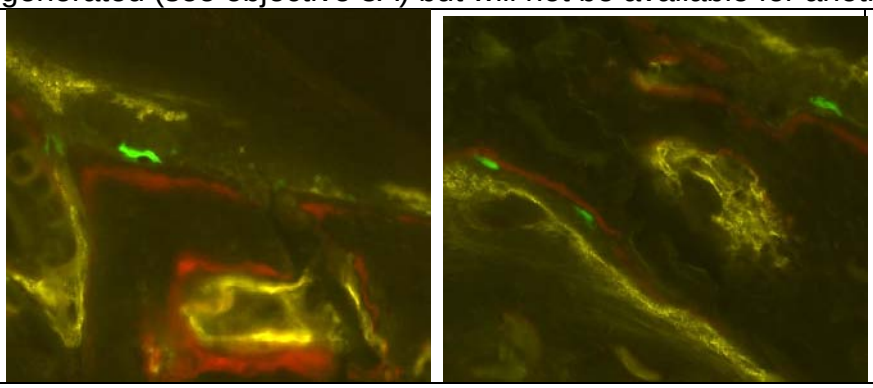

Figure 5: High power images along the upper surface of the right defect where the Col2.3GFP positive cell were observed. The yellow stain is ELF97 staining for osteoblastic AO activity much of which overlies the red alizarin complexone mineralization line. The GFP cell do not show AP activity and appear to lie between the AP+ and red mineralization line.

Subsequently the same slide was stained for a human specific mitochondrial antibody, which indicated that the cells above the bone were human in origin (figure 6). All of the osteoblastic cells within the bone structure either within the mineralized matrix or on top of a mineralization label lacked the human label. Instead the thin cells above the bone and the more rounded cells closes to the bone are strongly positive for the human antigen.

The human cells closest to bone acquired a different morphology than the “blastema like” cells with some having a hyperchondrocytic appearance. This transition zone has been difficult to characterize (figure 6B, panel A). While the mineralized matrix contains a relatively well-defined mineralization line, it does not have a corresponding strong line of AP activity (panel B). The human cells in this region do not appear to be AP positive. A safranin O stain for chondroitin sulfate characteristic of a cartilage matrix was negative but instead generated a blue color more characteristic of osteoid (panel D) and this region does show a diffuse alizarin complexone signal. More work needs to be done to better characterize the interface between the human “transition cells” and the underlying murine bone, but the evidence to date does not support the conclusion that the hES cells derived from the E->M cell culture protocol generated bone.

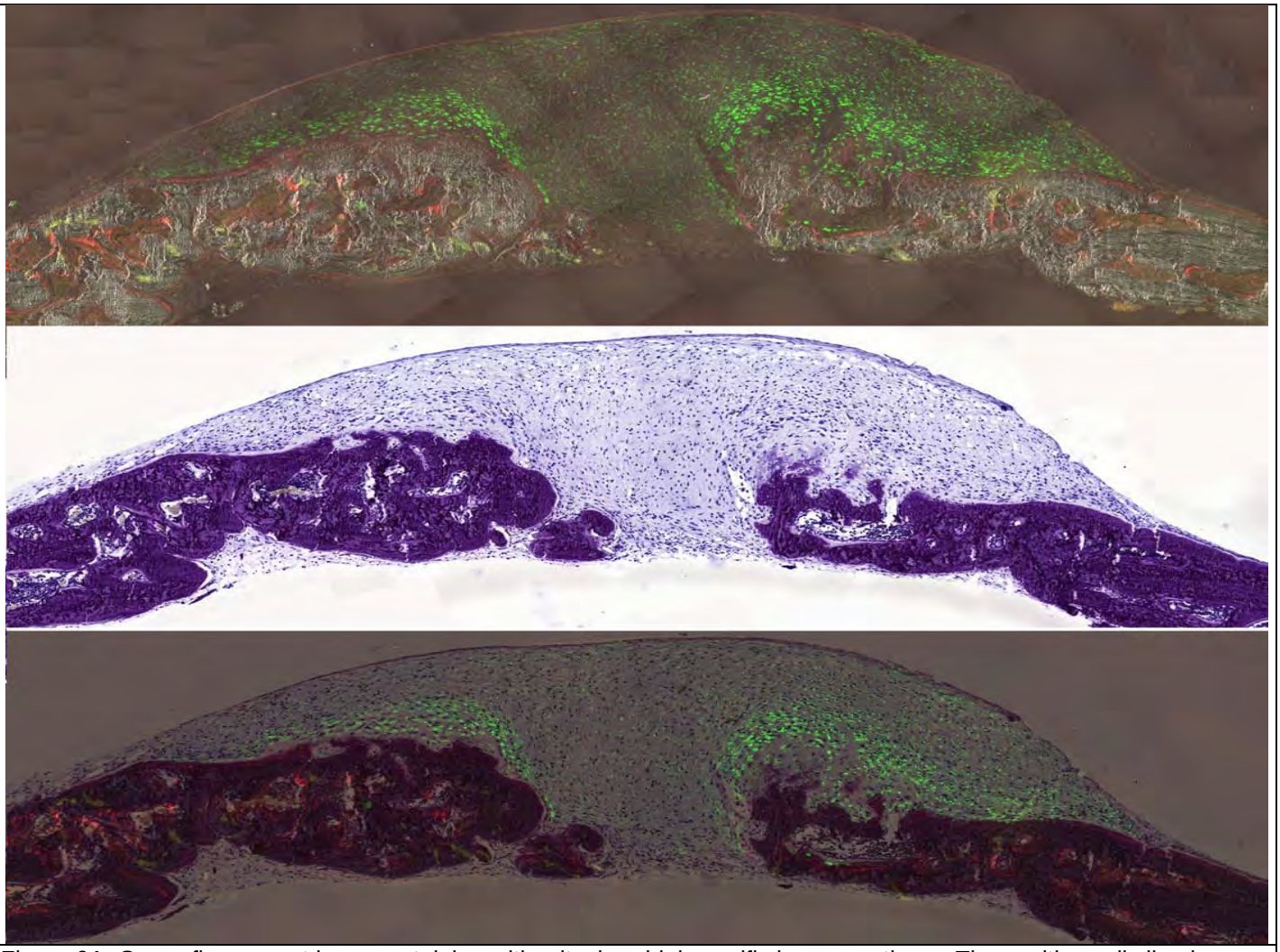

Figure 6A: Green fluorescent immunostaining with mitochondrial specific human antigen. The positive cells lie above the in growing bone. The cells within the bone are not positive for the Hu antigen. We are confident that we can detect human derived osteoblasts in mineralized sections of bone, because the bone formed within an iPS derived teratoma is reactive to the Hu antigen stain, is associated with recent mineralization and is strongly AP positive

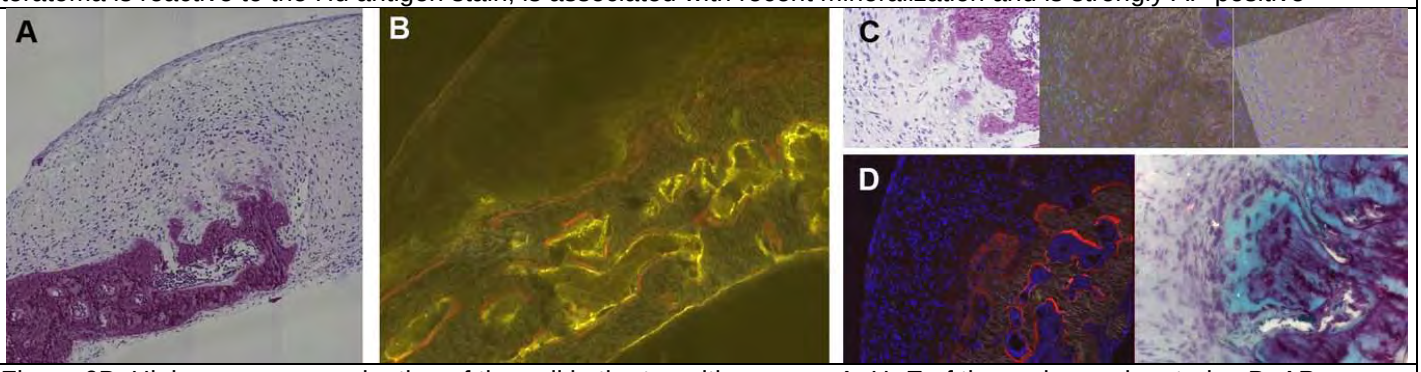

Figure 6B: Higher power examination of the cell in the transition zone. A. H+E of the region under study. B. AP (yellow) and red mineralization lines showing minimal activity in the transition zone. C and D. The area of matrix accumulation next to the well formed bone. A diffuse red mineralization is present in the region where the blue extracellular matrix has accumulated. Some of the cells in this zone may carry a Hu label but the level of differentiation (bone or cartilage) remains to be determined.

C. Implications for future research

Clearly the primary determinant for bone formation in the calvarial defect model is the quality of the osteoprogenitor cells that are introduced into the repair site. Our experience to date,

Figure 7: Biospherix instrumentation. It consists of two bays (manipulation and imaging) and atmosphere controlled modules located within a standard warm temperature incubator.

particularly in the mouse, is that robust progenitors can be obtained from primary BMSC cultures, but this capability is rapidly lost with cell passage. Because of the reports suggesting that low oxygen cell culture conditions was conducive for maintenance of progenitor activity, we requested and received a supplement to purchase and begin to use a low oxygen incubation (Biospherix, figure 7). That equipment has now been installed and we are learning how to take advantage of its capabilities. Avenues we are pursing (and the projected funding sources) include:

1. Murine progenitors – This work will be continued using R01 AR052374.

• The SMAA population that develops in the BMSC culture and has multi-skeletal lineage potential will be our primary focus. While low oxygen does not appear to enhance its growth in primary culture, we do have preliminary data suggesting the FAC sorted SMAA cells will continue to expand and retain progenitor potential when grown under low oxygen. We have developed a rapid hematopoietic depletion step of adherant BMSC cultures for FAC sorting and will utilize that step to harvest SMAA+ cells directly for plating to determine if that step can avoid a costly FAC sorting step.

•SMAA positive cells are still a heterogeneous population with microarray markers of bone, tendon, cartilage and adipocytes. To discriminate a bone progenitor from other candidates in the mixture, cell that are double positive of SMAA (red) and Osterix (green) are being isolated and tested for their osteogenic potential relative to SMAA positive cell lacking this marker combination. Our goal is to define to most restricted osteogenic cell for expansion and transplantation.

•Within the SMAA postive population there is a strong signal for Dkk3, a member of the noncanocial wnt inhibitor family that would not have been anticipated in a bone progenitor population. A Dkk3-eGFP reporter was acquired and it appears to mark a cell population in the periosteum (see Objective 2B) as well as a distinct subpopulation of cells completely independent of a bone nodule. The potential role of these cells for constraining the osteogenic activity to the bone surface and clinical use as an treatment for heterotopic ossification is developed in objective 2B).

•The microarray studies of SMAA positive cells also showed strong CTGF expression. CTGF-GFP positive cells were highly expressed in non-osteoblastic cells lining the trabeculae of the primary methaphysis, a site of active new bone formation. These CTGF+ cells can be isolated directly from bone marrow and the majority of these cells become SMAA positive by day 3 of cell culture. We need to understand the meaning of the CTGF+ cells and whether they could be used to isolate progenitors directly from fresh marrow aspirates without having to go through a cell culture step.

2. Human progenitors – to be continued with the 2010 earmark.

•Adult osteoprogenitor cells (1) – We have access to filtrates of bone marrow aspirates used for bone marrow transplantation that had been the practive in the late 1990's. The filtrates contain small pieces of bone and tissue that were directly frozen in LN2 and when thawed generate a lawn of fibroblastic like cells. The second passage of these cells produce genuine bone nodules and we

are currently testing their ability to make bone in vivo. If they prove to be osteogenic in vivo, then they will be the starting source of cells for progenitor expansion and enrichment using the low oxygen conditions.

•Adult osteoprogenitor cells (2) – Because a continued source of progenitor from marrow filtrates will not be available, we need to develop a reliable method for direct harvest from living subjects. We are in discussion now with members of the orthopedic department to acquire fresh marrow and associated trabecular bone fragments from which to generate low passage stromal cell cultures for further expansion under low oxygen conditions.

•Osteoprogenitor cells from hES and iPS cells – Ultimately hES and iPS cells will be the source of choice because of its potential for generating an unliminted number of progenitors with a prolonged regenerative capability. Defining a differentiation protocol for generating these progenitors will not be straight forward, but the adult stem cell work will give us direction and confidence that we can recognize osteogenic differentiation when it does occur. The hope is that once limited differentiation is achieved, then the method can be incrementally improved to become as robust and reliable as cells from adult tissue sources.

In summary, the calvarial defect model has proven to be an important test platform for assessing the bone progenitor potential of a test population whether it be murine or human in origin. The steps we will be taking to further improve the interpretative power of the histology will be discussed in objective 3. It's role in assessing scaffold biocompatibility with bone progenitor cells will continue to be the first line of in vivo evaluation. The advances that are envisioned to enhance the through put and interactions with the material science investigator that utilize this platform will be discussed in objective 3.

Objective 2A: Establish the long bone fracture/repair model

The objective of his project is to understand the cellular elements of normal fracture repair utilizing a series of the GFP reporter mice so that we can better understand the how a segmental defect of bone either heals or fails to heal (see objective 2B).

A. Knowledge gained over the life of the grant.

This project has be performed entirely by a orthopedic fellow, Dr. Chikara Ushiku, under the guidance of Dr. Douglas Adams and a publication of this work is in press. Dr. Ushiku has returned to Japan and his clinical practice of orthodpedics, although he hopes to establishing a research laboratory there. Utilizing mice harboring multiple GFP reporters that identify cells at different levels of osteoblast differentiation, he examined a closed tibial fracture model at increasing times after fracture induction. The important point that emerged from this study that was not appreciated by the field in general (figures in appended paper). Three phases of repair can be appreciated:

Phase 1: proliferation, migration and differentiation.

•With in one day after fracture evidence for progenitor activation (onset of SMAA-red expression) is evident within the inner layer of the periosteum at a surprising distance from the fracture site. At the same time, the periosteal bone lining cells which can be identified by solitary expression of an osteocalcin (Oc) reporter construct, begin to co-express the Col3.6 reporter.

•By day two, proliferation of the SMAA-red population within the periosteum is evident in association with a dissolution of a distinct outer periosteal layer. The bone lining cells now strongly express Oc and Col3.6, are positive for BSP expression by in situ hybridiztion (ISH) and have changed their morphology (thin to elipsoid) and orientation to the bone surface (parallel to angulated). These changes are associated with a transient expression of Oc-GFP in a thin layer of underlying osteocytes.

•By day 4, the SMAA population has greatly expanded in depth and has migrated centrally toward the fracture zone. Usually by this time the entire fracture zone is filled with the myofibroblastic-appearing SMAA positive cells the vast majority having originated from the periosteum although there may be some contribution from the overlying skeletal muscle. The bone

lining cells produce a intracellular matrix that begins to accumulate mineral. This region is contiguous with early Col3.6 only rounded cells that have developed from the SMAA progenitor cells. This junction between the bone lining cell matrix will anchor the developing bone of the outer cortical shell to the surface of intact cortical bone.

•Between day 4-7, the three differentiate structure of the early fracture are established. The bone that initially developed above the matrix made by the bone lining cells migrates forward toward the fracture zone and upward over cells that fill the fracture zone. These cells trail the advancing SMAA+ cells and differentiate from the SMAA+ cells. The transition from SMAA+ only to SMAA+/Col3.6 double positive cells is associated with a postive ISH signal for FGF2, BMP2 and VEGF. The SMAA+ cells within the fracture zone acquire chondrocytic morphology and express both Col2A1 and Col3.6 characteristic of fibrocartilage. A new thin layer of elongated cells is established over the surface of the developing bone that will establish the reconstituted periosteum.

Thus this early phase of proliferation, migration and differentiation is the crucial cellular foundation for successful fracture repair (see next). The SMAA+ multiprogenitor cells need to populate all of the subsequent structures (bone, cartilage, periosteum) the will provide the structural support and protective environment for bone repair without off target effects such as heterotopic ossification or pseudoarthrosis. The importance of a sufficient number of multipotential progenitor cells within the repair zone indicates that a segmental bone repair strategy has to deliver these cells during the earliest stages of the repair to replicate the temporal and spatial steps that lead to successful fracture repair.

Phase 2. Cartilage resorption and formation of the outer cortical shell.

•The cartilage forms in the center of the fracture zone which is the region of least vacularity. Presumably its function is to provide temporary stabilization of the defect until osteoblasts and blood vessels can enter the area. Between days 7-10 the cells activate a ColX-GFP reporter and areas of diffuse mineralization develop. At this point there is no invasion by blood vessels or osteoclasts.

•The immature osteoblast that develop adjacent to the chondrocytes appear to invade as channels between the chondrocytes. These cells form the initial diffuse mineralized osteoid over the chondrocytes structure and appears to be the target for the initial osteoclasts and attendent blood vessels. Between day 10 and 21, it is the continued osteoblastic channeling that initiates the osteoclastic resorption of the fibrocartilage and replacement with bone marrow. During this time osteoblasts differentiation advances over the surface of the cartilage but beneath the developing periosteum so that by day 21 an outer cortical shell, well anchored to the cortical bone at the base of the arch, provides the major structureal support of the bone.

Thus the success of the fracture repair depends on the ability of osteoblasts to continue to differentiate alone the outer margin of the cartilage and to direct the degradation of the fibrocartilagenous core of the fracture callus. The early osteoblastic cells are direct discendants of the SMAA+ cells which are at the leading edge of the advancing osteoblasts. This is a relationship that will have to be repeated in an engineered skeletal repair.

Phase 3: Inwarding of the outer cortical shell

•By 3 weeks the outer cortical shell is well formed and is actively making new bone on its inner surface. These osteoblasts have a more mature phenotype, being strongly positive for Oc and Col3.6 and generating a distinct mineralization line. On the outer surface of the formed bone, but beneath the periosteum, is a line of osteoclasts. This process of bone formation on the inner surface and bone resorption on the outer surface (similar to inwarding that remodels metaphyseal bone to diaphseal bone) gradually remodels the outer cortical shell toward the cortical bone.

•At the same time the outer cortical shell is being remodeled inward, osteoclasts are degrading the cortical bone that lies underneath the cortical shell. Presumably mechanical forces

have a major impact on the growth and remodeling of the outer cortical shell while the lack of forces on the bone beneath the shell is responsible for its resorption.

The model has been carried out for 12 weeks and the bone is not completely healed. Perhaps this is related to the continued presence of the internal support pin or may be a consequence of mice living in a confined cage. However it suggest that complete healing of an engineered defect will require that the repair region will require mechanical loading as well as a continued source of osteoblasts to drive the remodeling process.

B. Progress over the past year including the 1 year extension: the Dkk3 lineage.

We were able to recruit a replacement for Dr. Ushiku who also is an orthopedic surgeon (Dr. Mori Yu) interested in the cellular basis of fracture repair. His initial effort was to understand the earliest cellular events within the periosteum with a particular focus of the Dkk3+ cells that were

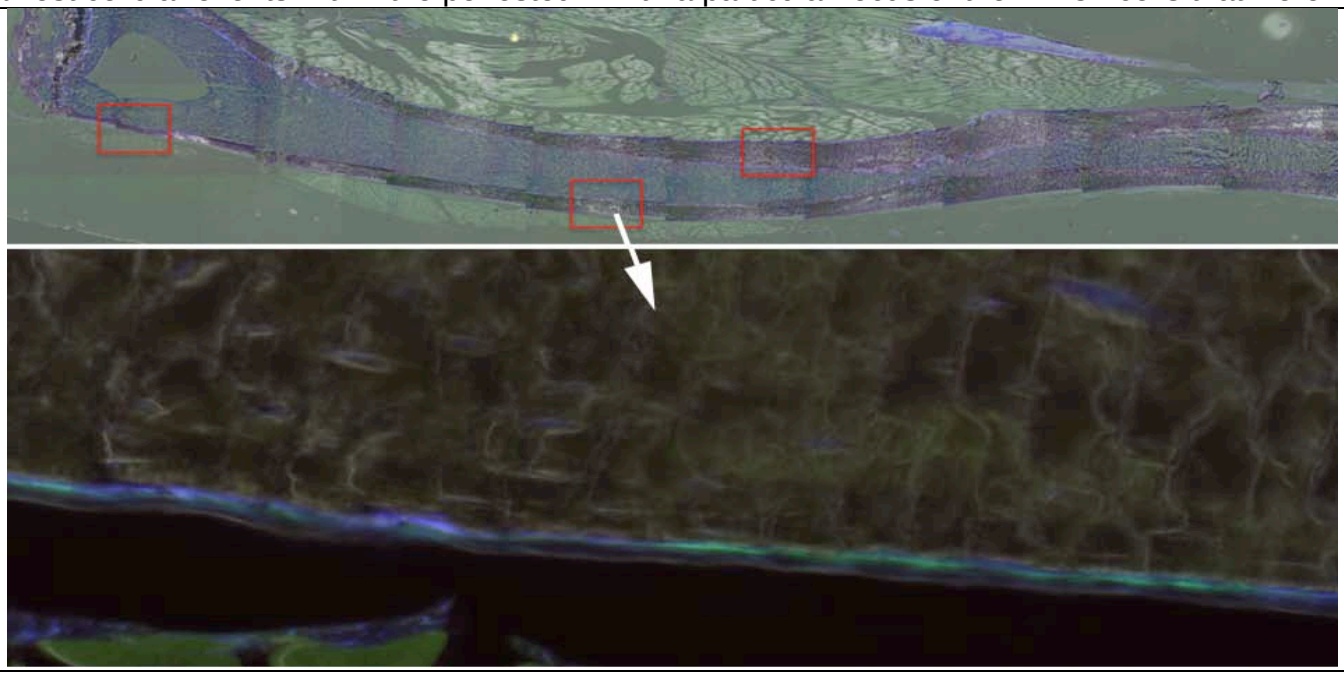

Figure 8A: Expression of Dkk3 green and Col3.6blue cells of the resting periosteum in the adult animal. The Dkk3green cell lie external to the Col3.6 bone lining cells but internal to the tenascin+ elongated periosteal cells.

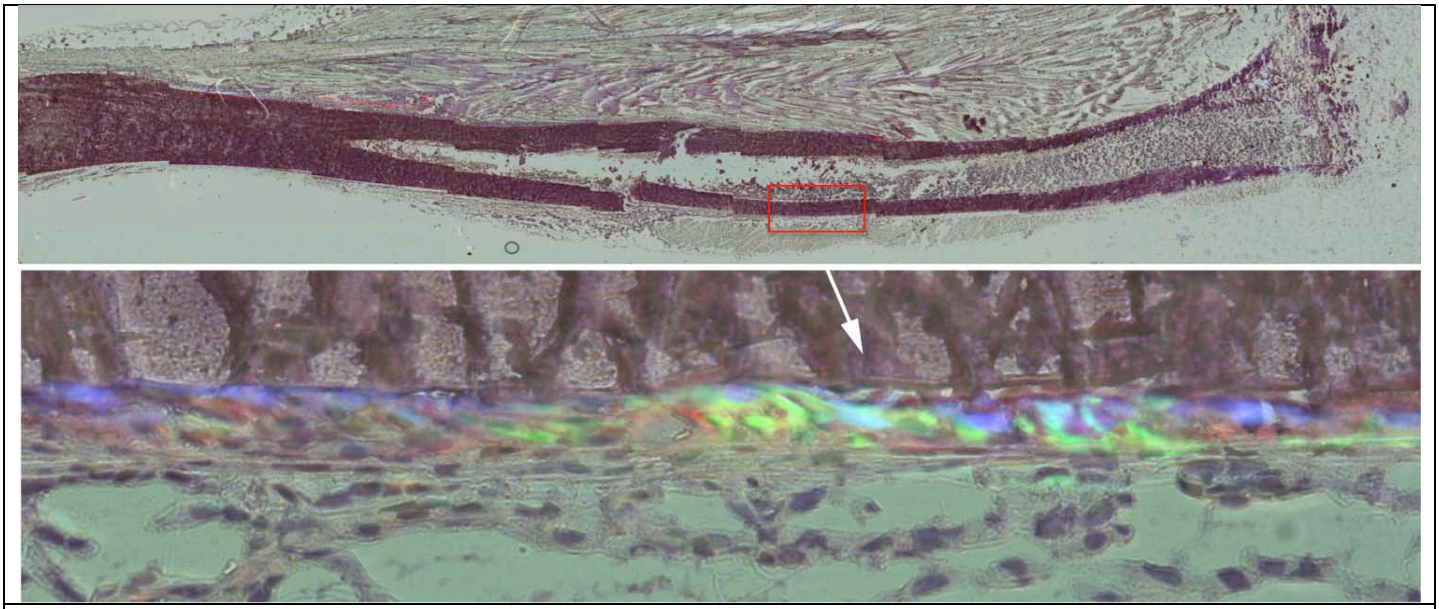

Figure 8B: Periosteum 2-3 days post fracture: The expanded cellular periosteum show admixture of SMAA-red progenitor cells which also express Dkk3green, Col3.6blue or both colors indicating the origin from a common progenitor cells within the periosteum.

identified in the BMSC cultures. Because these cells also carry the SMAA+ marker, we reasoned that they should be present in the population of progenitors that develop during the early fracture. This proved to be the case. In the unperturbed adult bone, occasional Dkk3 green cells can be observed on the periosteum overlying a Col3.6blue resting osteoblastic cells (figure 8A), although the Dkk3 reporter is strongly expressed in ligaments and tendon insertion sites. However 2-3 days after fracture a large expansion of Dkk3+ cells develop in the proliferative population on the cortical bone surface that are initially admixed with weak Col3.6 cells (figure 8B) both of which also express SMAAred. As the periosteal cells expand in number and migrate toward the fracture zone,

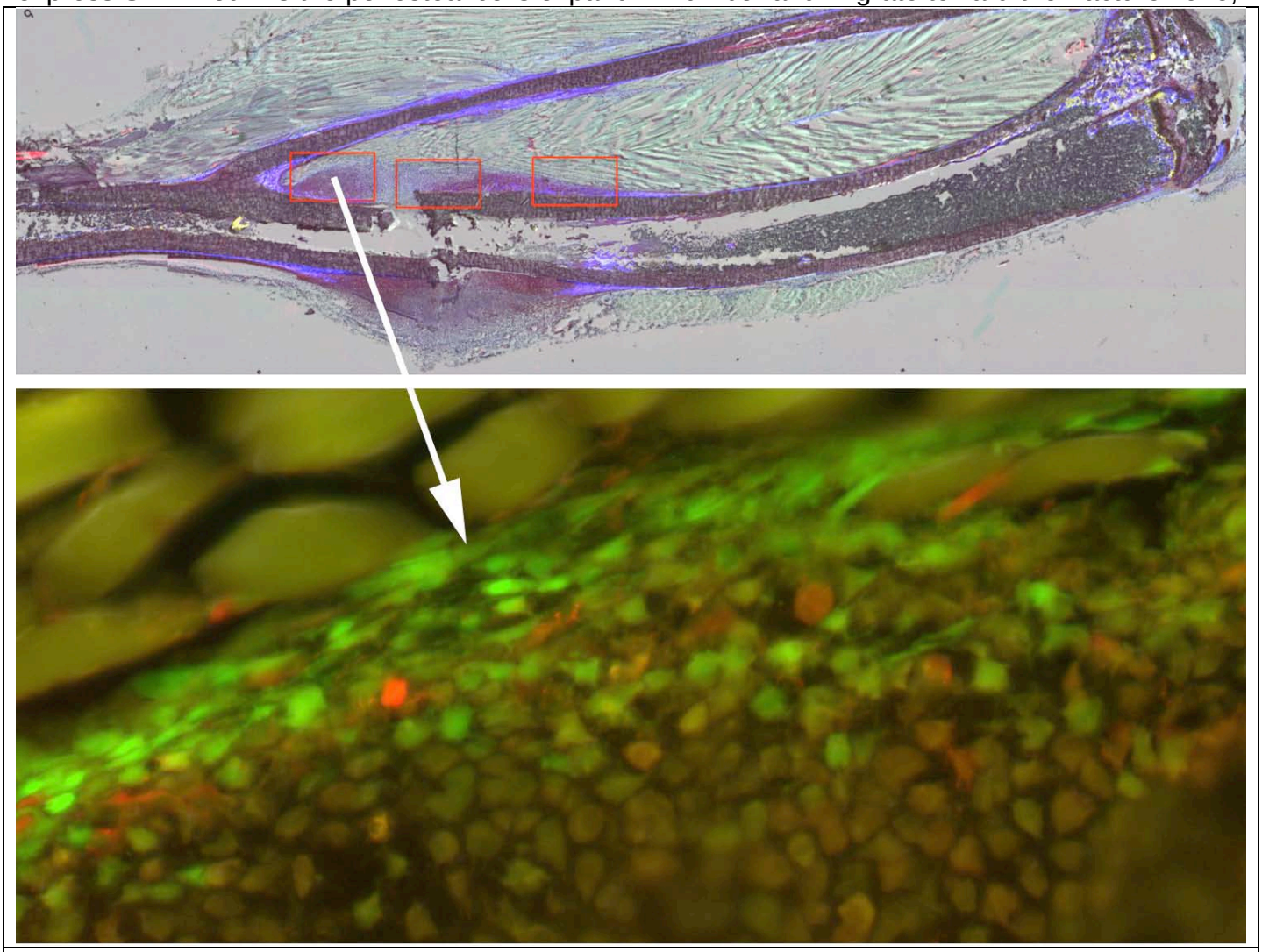

Figure 9: Developing fracture calls at 5 days post fracture. Top panel show the strong Col3.6 blue located primarily at the base of the developing callus and the central cartilage core that has developed within each side of the progenitors that are now filling the facture zone. The lower panel shows how the Dkk3 positive cells lie over the differentiating cartilage cells and exhibit either an elongated or rounded morphometry.

the Dkk3green and Col3.6 cells separate as two distinct cell populations. The Col3.6blue cells remain at the base of the developing callus to form the initial bone while the Dkk3+ cells extend over the differentiating chondrocytic cells (figure 9 top). Higher power examination of the Dkk3 cells show a gradient of morphometry with elongated cells at the outer surface and cells with increasing rounded shape on the inner surface (figure 9 bottom). The rounded chondrocytic cells also express Col3.6 blue and transiently express Col2A1-GFP as they rapidly differentiate into hypertrophic chondrocytes with strong Col10A1 reporter activity. This sequence of progression of reporter activity of SMAA -> Dkk3 -> Dkk3/weakCol3.6 -> Col2A1 -> ColX is characteristic of all the fibrocartilagenous structure we have examined (TMJ, enthesis, costal cartilage, intervertebral disc) and suggest to us a lineage relationship that needs further exploration. It is distinct from articular

cartilage and endochondral cartilage in that neither expresses SMAA or Col3.6. We feel that this type of evidence indicates that all chondrocytes are not the same and that different types have evolved for a different physiological purpose.

For example, when a section at the early stage of callus development is stained with antiColIV antibodies, a marker of endothelial basement membrane of invading blood vessels, one gets the impression that the Dkk3 cells provide a barrier function for vascular ingrowth to the underlying chondrogenic cells (figure 10, right) and possibly to provide a separation of the osteogenic activity from the overlying skeletal muscle (figure 10, left). Other antibody stains such

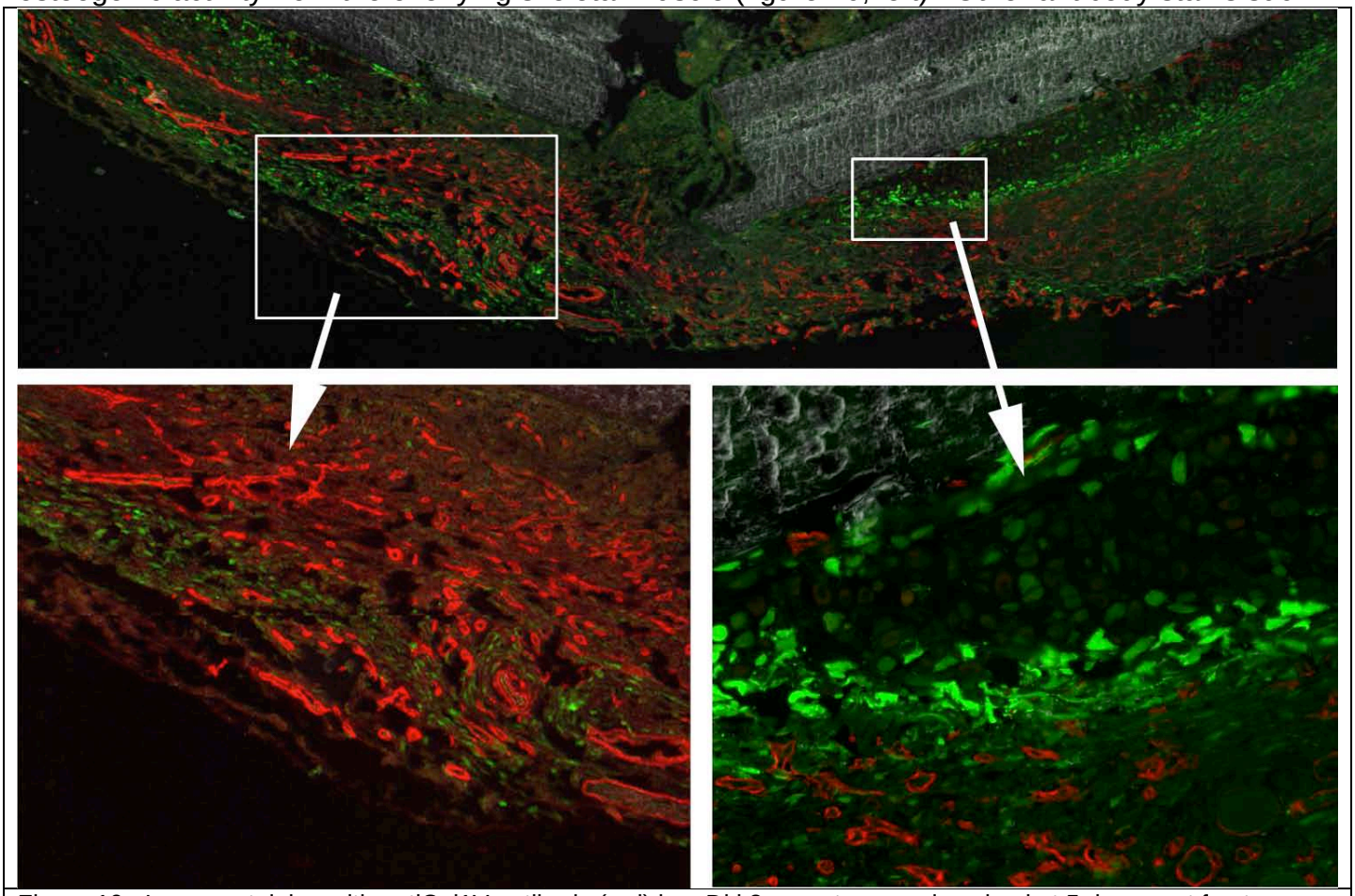

Figure 10: Immunostaining with antiCol1V antibody (red) in a Dkk3green transgenic animal at 5 days post fracture. The left panel show the elongated cells on the outer side of the developing callus while the right panel shows the Dkk3+ cells that overlie differentiating chondrocytes. In both cases, the presence of the Dkk3+ cells excludes immunostaining for endothelial cell basement membrane.

as fibronectin show that the Dkk3 cells are the only cells in the developing callus that do not express fibronectin (image not shown) and thus creating an unfavorable environment for vascular invasion or osteogenesis.

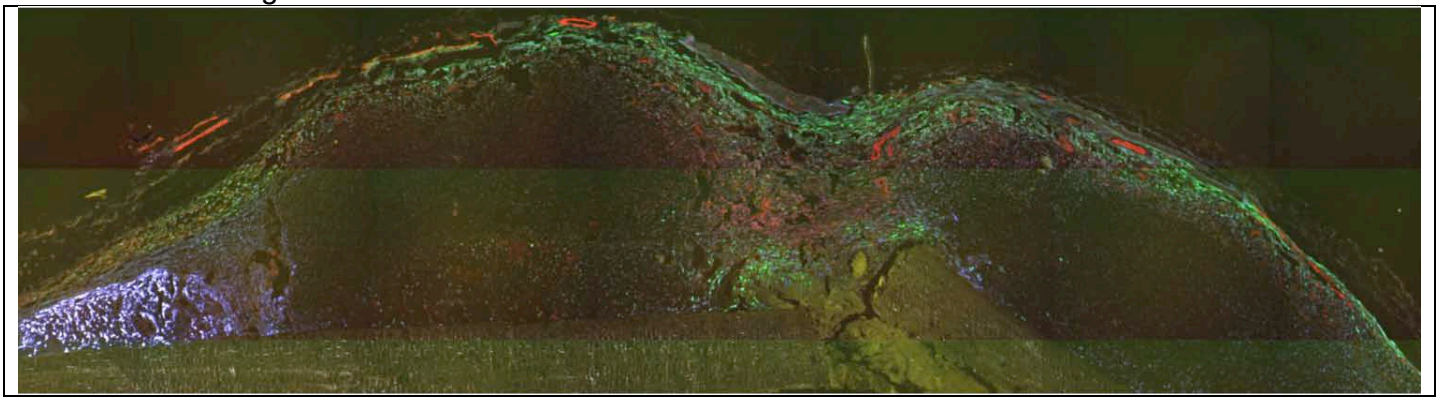

Figure 11: Expression of Col3.6blue, Dkk3green and SMAAred at day 7 of fracture. The cartilage core no longer expresses DKK3 although weak Col3.6 is evident. There is strong Col3.6 expression with bone formation at the base of the callus. Dkk3 extends over the surface of the developing callus and into the yet to differentiate interchondrogenic zone . By day 14, after the cortical bone have formed, most of the DKK3 activity will have disappeared.

As the callus assumes in fully differentiated state, the elongated Dkk3 cells seen in figure 9 will eventually reform into a periosteum that lies external to the outer cortical shell (figure 11). It's expression rapidly down-regulates as the outer bony cortical shell forms and inwardly remodels.

C. Implications for future research

The tibial fracture model, when utilized in the GFP reporter mice, has proven to be a rapidly produced and highly reliable platform for understanding the cellular and growth factor relationships that lead to an orderly repair of a bone fracture. The spatial and temporal events are rigidly structured and if we can understand them it will provide direction in how to devise skeletal repair strategies. Examples that may have clinical relevance include:

•In addition to its transient expression in the early fracture callus, Dkk3+ cell are highly expressed in the resting tendon/bone insertion site and articular cartilage, two regions that must resist ossification. Thus by implication, the Dkk3+ cells are associated with the ability to resist ossification. Knowing how this is accomplished may have therapeutic implication for heterotopic ossification as well as understanding diseases of articular cartilage and tendon associated with abnormal bone formation.

•The spatial expression of BMP, VEGF and FGF2 indicate that they are expressed by the early differentiating osteoblasts and not the proliferative and highly migratory SMAA+ only multiprogenitor cells. The impression given by the histology is one in which the SMAA+ cells furtherest from the osteogenic front are excaping from the effects of the growth factor while those closest to them cease their migration and are directed toward osteogenesis. This creates a wave for forward migrating progenitors and trailing immature osteoblasts that continues until the fracture space is filled and early differentiation is completed. The directionality may have implications for skeletal repair based on BMP delivery. If BMP is delivered into a site that is being filled with SMAA+ progenitors, it may hault the further inward migration by inducing differentiation of the front wave of progenitor cells. This would predict that a shell of bone would be observed surrounding the delivery vehicle, but few cells with this border including chondrocytes (see x). A better strategy would be to allow the progenitors to migrate into the defect area first and once in place release the BMP to promote differentiation. This is a concept that I will work with our material science group to investigate.

•The Dkk3+ population appears to inhibit the onset of ectopic ossification in muscle surrounding sites of bone repair as well a promoting fibrocartilage to initially stabilize the defect. We need to understand what factors these cell secrete to inhibit osteogenesis at unwanted places within the fracture environment. Potentially these factors might have therapeutic benefit to mitigate heterotopic ossification in a major trauma field.

Objective 2B: Gain experience with the long bone segmental defect

This work has been done by Dr. Liping Wang, the research associate who has performed all of the animal surgery for my group as well as for the material sceintists. For the past 18 months he has tried a number of stabilizing techniques and we have compared our result with those from Dr. Lieberman's group that uses external fixation. Although we are still learning how to interpret the histology from the various experimental surgical models, we feel that certain observation appear to be constant.

A. Knowledge gained over the life of the grant

The experimental surgical protocols appear to have a large influence on the ability of a segmental defect to spontaneously heal. Known variables include the size of the defect, the stability of the fixation and adequate vascularity.

•External fixation impedes the periosteal response to bone formation. The rigid C-support developed by Dr. Wang was effective in maintaining defect stability, but a very disorganized periosteal response failed to generate a cortical bridge (figure 12A). In addition the figure illustrates when the scaffold is loaded with mCOB cells the periosteal response is even less than scaffold alone. This speaks to importance of using the appropriate type of progenitor cell for long bone repair. mCOB cell produce a membraneous bone that does not integrate will with surrounding host bone.

Figure 12A: Segmental defect healing using the C-clamp external support with or without addition of mCOB cells to the repair region. There appears to be even less periosteal activity in the bone given the mCOB cells.

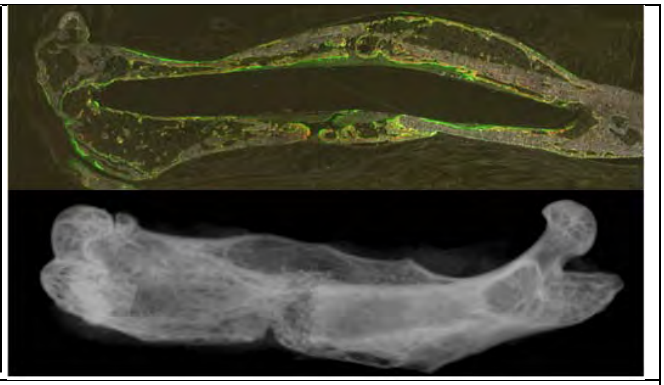

Figure 12B: Spontaneous repair of a segmental defect stabilize with the internal plastic pin (6 weeks post surgery). The mice carry the Col3.6green reporter. A well developed outer cortical shell is evident.

•Internal fixation with a plastic (polycarbonate) pin does allow for development of the periosteum and an outer cortical shell (see figure 12B and last year's report). However when the animals are subjected to total body irradiation in preparation for progenitor transplantation, the periosteal response is greatly inhibited. The donor cells do make bone but primarily as a collar of cells that line the support pin, which appears to join the exposed ends of the diaphyseal bone. This finding indicates that transplantation studies for segmental defect will have to be performed in the immunocompromised mice that will accept a transplant without further disruption of the immune system.

B. Progress over the past year

• NOD-scid IL2rg null mice (NSG) became available during the final year and proved to be of sufficient size and stamina for the segmental defect model. The animal developed a strong periosteal response and outer cortical shell that was equivalent of our non-irradiated CD1 transgenic animals. Figure 13 illustrated a transplantation experiment using these animals as a recipient for Col3.6blue BMSC cells. Not only did the pin provide good alignment and was conducive for production of an outer cortical shell (6 week time point), but a secondary line of bone appears to have developed along the surface of the pin that extends between the ends of the cortical bone (Figure 13A). The histology (panels B and C) appears to show two forms of healing. Panel D show the formation of the outer cortical shell, which is highly populated with the donor Col3.6blue reporter with underlying mineralization line. Beneath the shell is a thinner line of active bone formation growing away from the plastic pin (some of the bone appears to have been lost in the histological section). Panel E shows that a layer of bone developed between the cortical ends of the defect along the margin of the plastic pin, and many of the osteoblasts making this bone is donor derived. This bone layer is thicker than the one underlying the cortical shell with formation extending from and toward the plastic pin. Thus the pin may not only provide a stabilizing role, it may direct how the progenitors cell are position along its surface in addition to for formation of the outer cortical shell. It may also prevent progenitor cells from developing a pseudoarthrosis (see later).

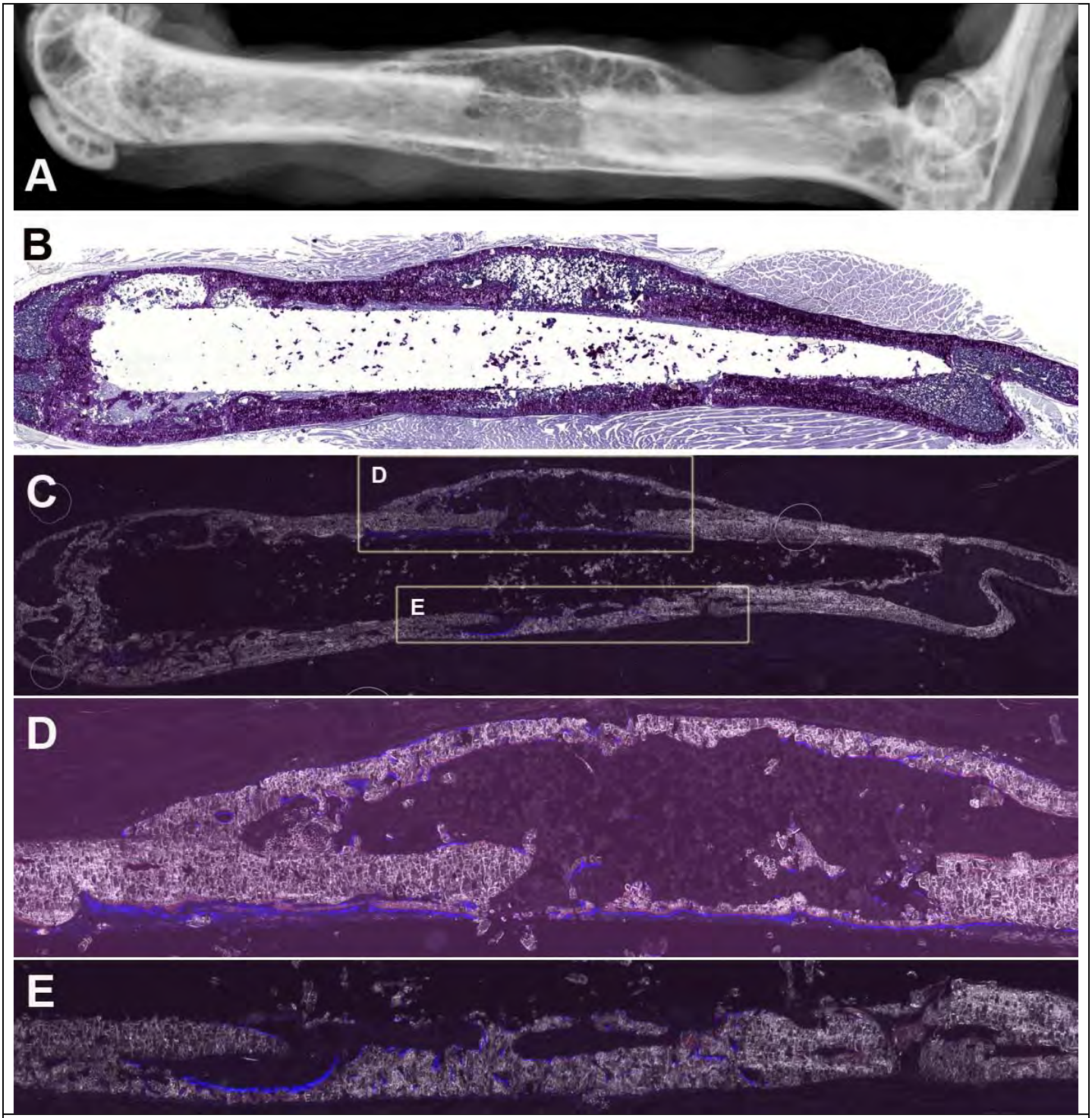

Figure 13: Healing of a segmental defect in a non-transgenic NSG mouse stabilized with an internal plastic pin and transplanted with Col3.6blue donor cells. A. Digital xray showing the outer cortical shell and the thin layer of bone that developed adjacent to the pin surface. B. H&E of the repair. C. Dark field and fluorescent image of the entire bone with the boxes showing the location of the enlarged images shown in panels D and E. The enlarged images show the participation of donor derived BMSC progenitors in both type of bridging bone formation.

•Early host progenitor events in the segmental defect model. The X-rays and histology of a successful repair show the formation of the outer cortical shell, which presumably develops from the periosteum by the same mechanism as a fracture. To test this assumption, Col3.6blue/Ocgreeen double transgenic mice were subjected with a 3.0 mm segmental defect that was supported by an internal plastic pin. The animals were sacrificed 7 and 14 days later (figure 14). Although somewhat less well developed than a fracture, by 7 days a periosteal Col3.6blue

population resided above an activated Oc-green bone lining cell population. By day 14 this population has expanded significantly and has progressed to full osteogenesis, but it has not

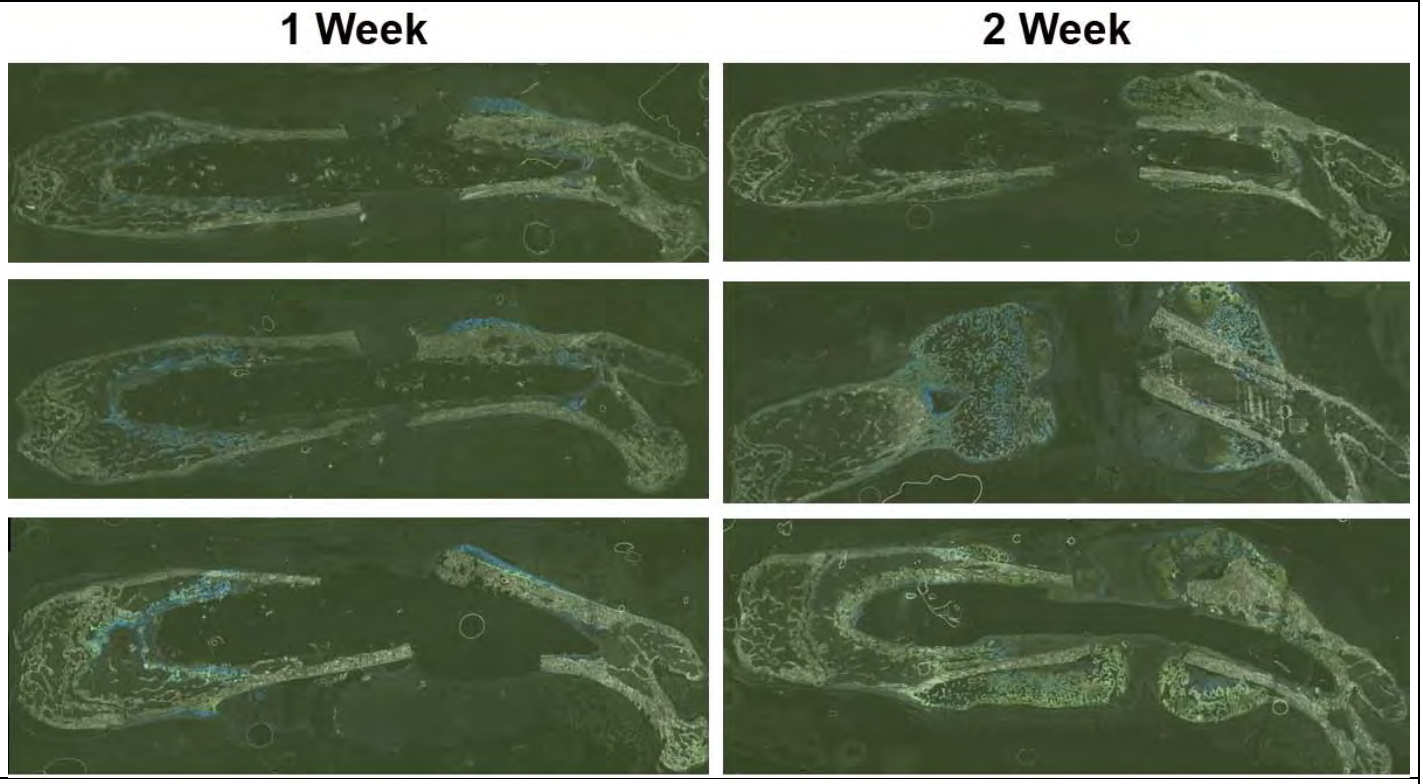

Figure 14: Progression of periosteal healing 1 and 2 weeks after induction. These low power scanning images demonstrate the Col3.6blue of the early differentiation osteoblasts (1 wk) and the yellow of tetracycling bone labeling (2 wks). High power images show the changes in the bone lining cells reported by the OCgreen reporter.

spanned the defect. Instead the defect region is across the ends of the gap is filled with fibroblastic cells suggesting that the progenitor potential of the advancing front has been exhausted. This is one potential explanation for the formation of a pseudoarthrosis that forms within a defect. The progenitors that fill a defect are unable to establish a stabilizing structure across the defect assume a disorganized differentiation process between the cortical end on each side of the defect. Although this cellular process will require more evaluation before it is clearly understood, it does appear the early stage of progenitor proliferation and migration into the defect areas is a critical step. It is necessary to fill a space that will become the outer cortical shell, but not allowed to fill the space between the ends of the bone at the expense of forming the nascent cortical shell.

C. Implications for future research

Two major determinants of a successful segmental repair need to be better defined:

1. type of stabilization – internal vs. external and its effect on how progentor cells are directed to site where new bone will be formed. This is a challenge that will involve mechanical and material scientists to formulate and test the most optimal design. Can a resorbable or removable internal support be developed. Will an external support that does not rely on wires that extend around the surface of the bone (transcortical pins attached to an extenal support) allow an adequate periosteal response to develop, or is the internal pin needed to prevent the progenitors from filling the space between the two ends of defect so that the progentor will be directed to form the outer cortical shell?

2. the number and quality of osteoprogenitor cells needed to form the outer cortical shell. What growth factors can be added to the defect site to enhance the expansion and migration of the progenitors into the defect space. When is the optimal time to add a differentiation factor since adding it prematurely will halt further migration. Is there an optimal time to add donor

osteoprogenitor cells? Is it best to use multipotential progenitors or should a mixture of committed bone, cartilage and periosteal progenitors be employed.

Both of these important consideration need further attention, but will require obtaining a new funding source to support the effort. Key to this work are the NSG mice and inbreeding of a bone and cartilage specific reporter to distinguish host and donor contribution the the repair. Figure 15A

Tg Embryos	->	rederive in NSG Females (F0)
Tg mice (F0) x NSG (F0)	->	F1 (select mice carrying GFP, all mice have equal distribtuion of CD1 and NSG)
F1-Tg x NSG	->	N1 (select mice with GFP; asymetry of genotype initiated)
N1-Tg x NSG	->	N2 (select mice with GFP and mice with greatest NSG gene load using DNA microarray, see analysis for mice with 75% NSG
N2-Tg(75%) x NSG	->	N3 (to be tested in October 2010)

Figure 15A: Breeding protocol to generate the GFP reporter in the NSG mouse line.

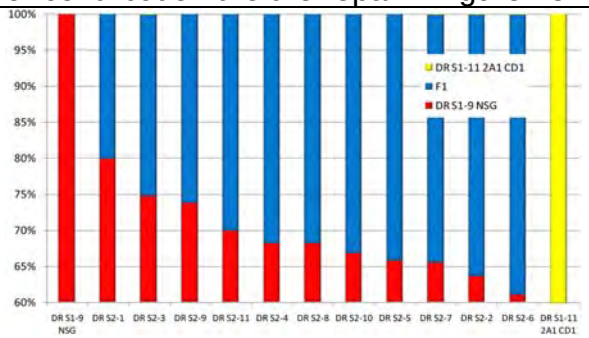

Figure 15B: First analysis of SNPs for NSG genetic background (red) and the loss of the CD1.

illustrates the progress that has been made. The transgene was introduced into the colony by embryo transfer so as not to contaminate the immunocompromized mice with flora from the transgenic line. The CD1 offspring, now carrying the flora of the NSG mouse line, was back bred twice with non-transgenic NSG mice and the N2 mice were tested by line specific SNPs for the relative contribution of CD1 and NSG (figure 15B). Mice in the N2 generation with greater than 75% NGS genetic load were selected for the next round of breeding. This process is called speed congenics and it is estimated to halve the number of back breeding necessary (from 10 to 5) to reconstitute the NGS genetic background. Thus it will be another year before these TG carrying NSG mice become available for use.

Objective 3A: Image analysis of repair lesions

A. Knowledge gained over the life of the grant

Our collaboration with Dr. Shin and Hong in the Department of Computer Science at UConn Storrs has been one of my most enjoyable scientific interactions of my career. Our weekly video conferences in which problems are identified and solutions found has given us confidence that our vision of computer based image analysis of skeletal biology is possible and it can be applied to a wide variety of normal and repair conditions. The fundamental basis of the our computer-based approach is:

•Generate multiple images of the same section in which each extracted fluorescent color has a biological meaning. Thus colors for mineralization lines, GFP for specific cell types, or substrate for a particular cellular activity (enzyme, immunostain or ISH) can be inter-related and mapped back to the mineralized surface of the section.

•One the images are obtained and pushed to Dr. Hong program, a pre-processing procedure is performed to vertically align the images with the use of registration beads that are embedded in the sectioning tape. This corrects for subtle changes in image alignment and shrinkage artifacts associated with the multiple stains and scannings.

•Using the image of the mineralized bone, a second preprocessing step establishes the region of interest (ROI) and defines the bone surface within the ROI. For bone histomorphometry of the femur or vertebra, this is determined based on the margins of the bone but we are still developing the rules for segmental defects of the calvaria and long bone.

•Thresholding each fluorescent signal as present or absent based on fixed criteria that are consistently applied across a sample set. No human judgment is made once the threshold is set. For this to be meaningful, all the tissue processing, staining and imaging is performed as batch

process. Much of our time has been spent developing the tolerances for processing that do not change the signal intensity within the sample batch.

•Mapping the multiple fluorescent signals to the surface of the bone (projection) allows the computation of mineralization and cellular activity as a percentage of bone surface. In contrast to the manual measurements and computation, which can amount to half of the total time for a histomorphometric analysis, the computer performs the measurement and calculation in minutes and generates tables of results and statistics automatically (figure 16). We have concentrated on

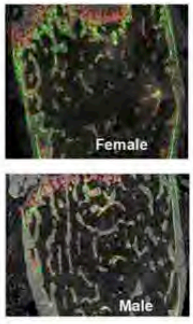

Comparison of Male vs Females in C57Bl/6 Mice

Static

		BV/TV	Tb.Th	Tb.N	Tb.Sp
Female	1	3.45	19.63	1.76	549.04
	2	6.06	17.11	3.54	265.16
	3	3.52	17.72	1.99	485.54
	4	7.53	18.08	4.16	222.09
	5	8.58	18.50	4.64	197.16
	6	6.99	16.26	4.30	216.41
	mean	5.72	17.84	3.24	342.66
	std	2.23	1.29	1.32	162.88
Male	7	14.96	33.63	4.45	191.16
	8	12.09	22.02	5.49	160.12
	9	14.60	26.05	5.61	152.32
	10	13.35	24.12	5.53	156.62
	11	10.60	23.43	4.53	197.55
	12	7.64	18.96	4.03	229.17
	mean	12.21	24.70	4.94	181.16
	std	2.76	4.97	0.68	30.17
p value: F vs M		**0.0010**	**0.0092**	**0.0211**	**0.0452**

Dynamic

		R/BS	G/BS	R_only/BS	G_only/BS	sLS/BS	dLS/BS	LS/BS	MS/BS	sLS/LS	dLS/LS	dLS/sLS	MAR(um)	BFR
Female	1	33.58	20.22	21.83	8.47	30.31	11.74	42.05	26.90	72.07	27.93	38.75	1.17	31.58
	2	36.94	21.18	21.93	6.17	28.11	15.01	43.11	29.06	65.19	34.81	53.40	1.04	30.28
	3	21.79	15.74	17.14	11.09	28.23	4.65	32.88	18.77	85.86	14.14	16.47	1.20	22.53
	4	34.91	0.00	34.91	0.00	34.91	0.00	34.91	17.45	100.00	0.00	0.00	NaN2	NaN2
	5	48.41	32.42	25.29	9.30	34.59	23.12	57.71	40.42	59.94	40.06	66.85	1.12	45.43
	6	41.52	23.60	28.66	10.74	39.40	12.86	52.26	32.56	75.39	24.61	32.64	1.07	34.87
	mean	36.45	22.63	22.97	9.16	32.13	13.48	45.60	29.54	71.69	28.31	41.62	1.12	32.94
	std	9.90	6.17	4.30	1.98	4.84	8.65	9.64	7.92	9.94	9.94	19.34	0.07	8.32
Male	7	36.19	10.42	30.64	4.88	35.52	5.54	41.06	23.30	86.50	13.50	15.61	1.08	25.06
	8	24.58	20.55	16.05	12.02	28.07	8.53	36.60	22.57	76.69	23.31	30.40	0.73	16.57
	9	27.60	16.44	20.17	9.01	29.18	7.43	36.61	22.02	79.70	20.30	25.47	1.00	22.05
	10	21.58	21.64	13.39	13.44	26.83	8.20	35.02	21.61	76.60	23.40	30.55	0.92	19.83
	11	37.25	27.31	23.56	13.62	37.18	13.70	50.87	32.28	73.08	26.92	36.85	0.71	22.87
	12	20.42	21.91	11.93	13.42	25.35	8.49	33.84	21.16	74.92	25.08	33.47	1.00	21.26
	mean	27.94	19.71	19.29	11.06	30.35	8.65	39.00	23.82	77.91	22.09	28.72	0.91	21.27
	std	7.25	5.73	7.03	3.50	4.84	2.72	6.31	4.21	4.74	4.74	7.45	0.15	2.89
p value: F vs M		0.0764	0.2208	0.1584	0.1438	0.2804	0.0936	0.1160	0.0988	0.1252	0.1252	0.1094	**0.0088**	**0.0160**

Figure 16: Results of a static and dynamic histomorphometric analysis for C57Bl/6 mice at 16 weeks of age comparing male vs female animals. Despite the low bone mass of the females, they have a significantly elevated bone formation rate. The methods used for histomorphometry are identical to those used to assess a skeletal repair defect.

establishing standards for histomorphometry of femur and vertebra in C57Bl/6 and CD1 male and female mice at 8 and 16 weeks of age. In both lines it is very striking the high level of bone turnover in the female mice at both ages (figure 17).

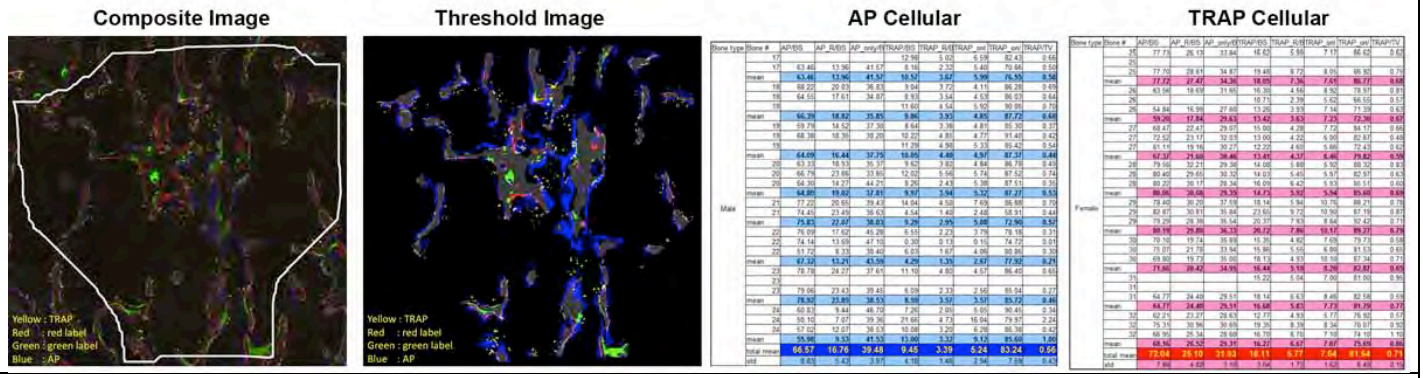

Figure 17: After the section is imaged for the fluorescent mineralization lines, it is incubated and image successively for TRAP and AP and the resulting images are co-localized with the previous obtained images. The left panel is the composite fluorescent image while next to it is how the computer detected the complex patterns of mineralization lines, AP, TRAP and trabecular bone. The analysis is tabulated to the right of the figure. The full analysis show that the female mice have significantly more bone surfaces lined with TRAP and AP positive cells consistent with the higher bone turnover than male animals.

B. Progress over the past year

Much of our effort was refining the quality and consistency of our sectioning technique that was require when a new technician (Ms. Chen) was hired to allow Dr. Xi Jiang more time to develop and trouble shoot new staining techniques. For example, we revisited the optimal dosing of calcein and alizarin complexone to achieve equal % bone surface labeling. Specific problems that Dr. Jiang achieved included:

•Using different formulation of chitosan prepared by Dr. Nair, an adhesive to permanently attach the tape to the glass slide was achieved that would tolerate the acid conditions used for the TRAP stain. This allows multiple stain and imaging steps to be performed on the same histological section (figure 17).

•Conditions for AP and TRAP staining that can be used to assess the cellular histomorphometry of a bone section. While the AP activity is robust and stable, TRAP is rapidly

lost at room temperature and requires long-term storage at -70ºC. The enzyme stain has to be recorded within 1-2 hrs after the reaction is initiated to achieve consistent levels of activity across a sample set.

•Distinguishing mouse and human cells in a transplantation experiment – A number of different antibodies were screened to identify a human specific (mitochondria) fluorescence-based identification probe (see figure 6A). We have not been successful in finding a mouse specific antibody. Peptide nucleic acids (PNA) are a rapid and sensitive hybridization probe amenable to high though put analysis and imaging (as opposed to standard nucleic acid probes). We had PNA probes made to mouse telomeres (they are much larger than human) and human Alu targets that carry a different fluorescent probe. The hybridization conditions that discriminate between the two cell sources are still being developed. This step will be an interim until the NSG-TG mice become available, but an immunological or hybridization protocol will always be useful for interpreting a transplantation study.

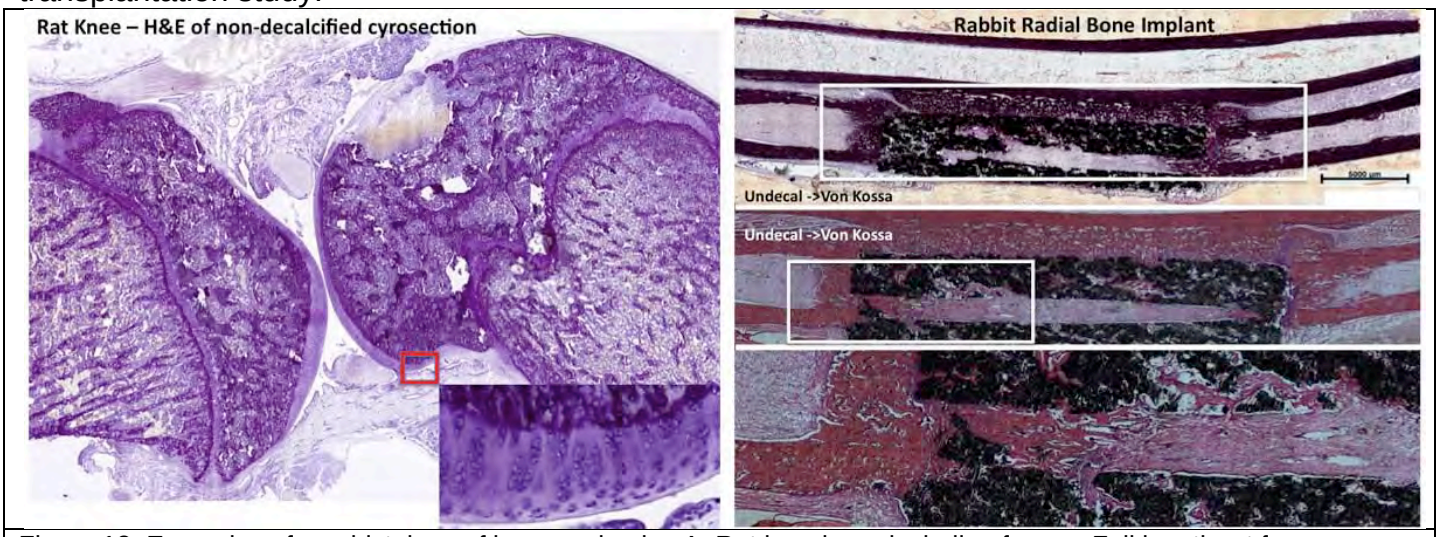

Figure 18: Examples of cryohistology of larger animals. A. Rat long bone including femur. Full length rat femur section, similar to those in mice are possible. B. Rabbit segmental defect in the radius. A 1.5 cm defect was filled with a ceramic insert and we cut a 2.5 cm section to flank the insert region. The upper panel is a von Kossa to show that the section is mineralized. A sister section was decalcified on the slide, stained and imaged to show the cellular detail by chromogenic staining.

•Applying the frozen histology to larger animal models – From other projects, we have had the opportunity to utilize the cryohistology sectioning and imaging protocols on larger, non-transgenic animals. Figure 16 illustrates the quality of sections on non-decalcified bone used on a rat joint (steel knife) and a rabbit radius containing a ceramic implant (tungsten blade). In the case of the rabbit bone, the section was 2.5 cm in length. The quality of the H&E image is very acceptable and the techniques for determining mineralization lines and AP/TRAP enzyme activity develop for the mouse should be readily applicable to larger animals. Thus the speed of processing and the power for fluorescent imaging should facilitate analysis of histology in larger animal models.

•Defining the ROI for image analysis of a segmental defect of bone – Last year's report demonstrated how the ROI for a calvarial defect is identified and used to assess the extent of new bone formed and the contribution of host and donor to the repair process. In concert with Dr. Lieberman's group, we are developing rules to perform image analysis of a segmental defect. Figure 17 illustrates the range of repair that is observed in the mouse defect that utilizes external fixation. Failure of healing either creates a closure of the end of the cortical bone or the end remains open (pseudoarthrosis). Healing is associated with the formation of a bridging structure.

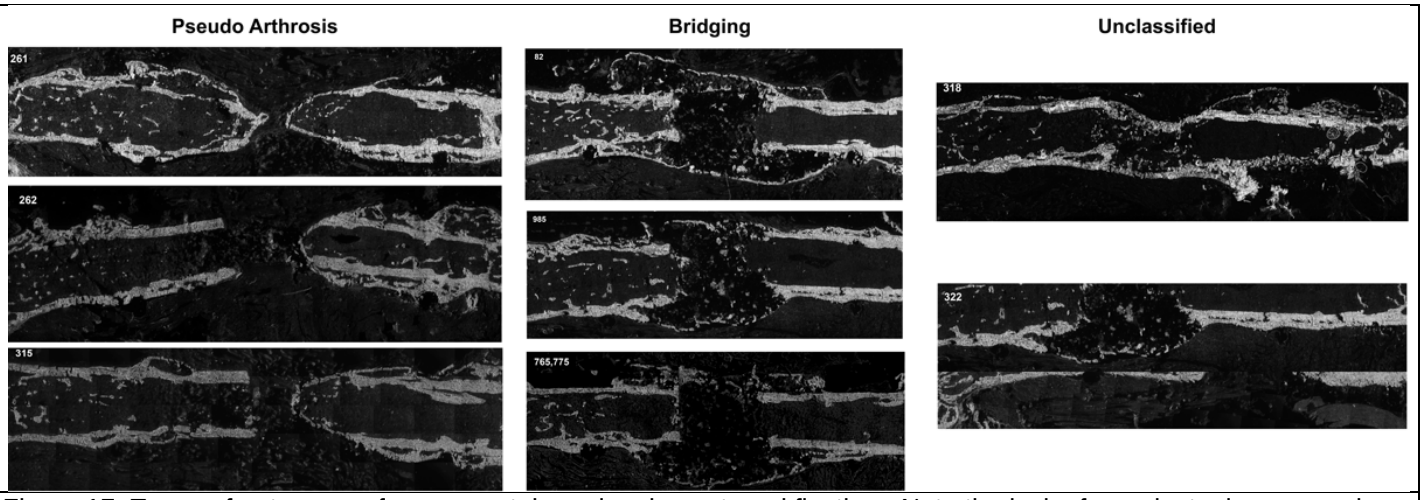

Figure 17: Types of outcomes of a segmental repair using external fixation. Note the lack of a periosteal response in the bones that developed pseudoarthrosis.

A third outcome is the formation of a cortical structure that is in line with the ends of the original bone whose resolution to healing or pseudoarthrosis is not yet established. As discussed above, the in-line structure is frequently observed with internal pinning. Our working model for defining these outcomes is illustrated in figure 18. By defining the bone that is formed above and adjacent to the ends of the cortical bone (ROI1), we can capture activity leading to healing of the bone. Thus formation of a bridge or cortical extension will be identified in this ROI and the continuity, thickness, and cellular contribution can be assessed. R0I2 captures activity that develops between the ends of the cortical bone. The ends can be wide open, partially or completely closed. Thus some expression of extent of activity of ROI1 to ROI2 will be a histological measure of the success of the repair. This is an active area of continued discussion at our Friday videoconference sessions and further modification can be anticipated.

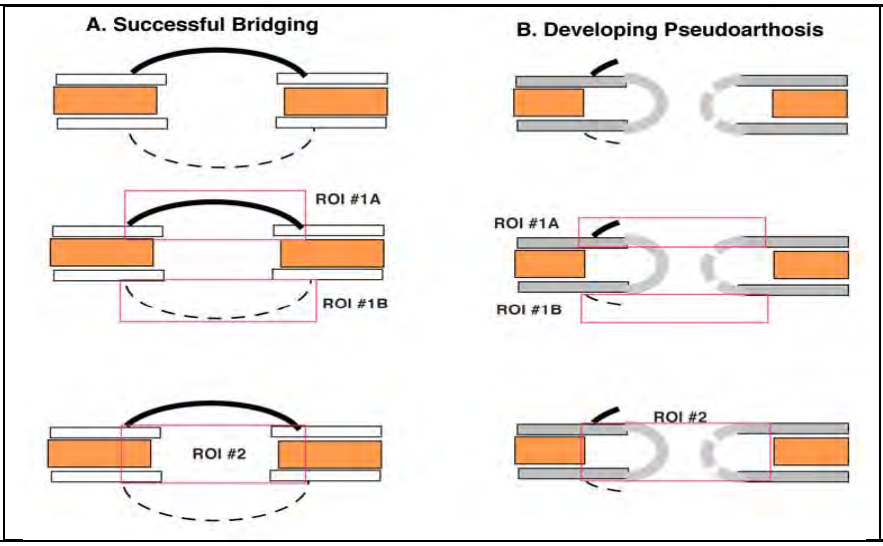

Figure 18: Defining the ROI in the segmental defect. ROI-1 is the region containing the outer cortical shell that is external to the cortical bone. The region on either side of the defect will be analyzed. ROI-2 is defined as the region contained within the cortical bone that flank the defect and extends to the margin of the outer cortical shell. Each structure can be continuous or fragmented and of variable thickness. Not shown is how to assess the bridging that occurs along the internal plastic pin.

C. Implications for future research

The ability to perform the frozen histology on mineralized bone from mice and larger animals open the possibility for computer based image analysis of skeletal repair on a variety of animal models. With the use of automated imaging and database management (see next), we are thinking about the possibility of a centralized processing and imaging facility that would be available to the skeletal engineering community. Such a facility, not only would speed through the choke point of traditional histology, but would be a way to compare the effectiveness of various repair strategies. We are in the process of obtaining a provisional patent on our

histological/analytical processes as the first step that has to be taken before an commercial service is developed to meet this need.

Objective 3B: Archiving and retrieving histological images

A. Knowledge gained over the life of the grant

The database that was designed to capture, archive and retrieve experimental details and visual results (Xrays, pictures, histology) was described in last year's report. It has been in use for almost 2 year and is continually being modified as we gain experience with the concept.

•Developing a naming and organization structure that is transparent between our database and the files we send to Storrs for image analysis is essential for coordinating the experimental data to the calculated outcome. An FTP site for managing the transfer of the large image files has been established to facilitate this process.

•Establishing a culture within the PIs and technicians to define an experiment within the database prior to performing the experiment has been a learning experience. However the defining process greatly increases the power of the experiment as well as the planning process. Everyone involved in the experiment understands their role and responsibility for entering their information into the database as it becomes available.

•As the data accumulates in the database, individual or group meetings are arranged in which comments and questions are annotated, and new approaches are planned. Because all members of an experiment have access to the database, they can review and comment individually as well as with the group. Composite images that could be used in a presentation (slide or manuscript) are also deposited for group usage. This communal approach to science is new to all of us and will require continued commitment to be usefull to all.

B. Progress over the past year

Figure 19: Mirax Midi

The biggest effort was setting up and learning how to use the Mirax Midi. This instrument is capable of automated 20X imaging of multiple large tissue sections on one slide. A loading cassette of 12 slides with multiple samples can be programmed into the machine for overnight unattended scanning. Thus we can deposit 3 sections per slide over 12 slides to do a complete histomorphometric analysis unattended. The technician has to define the field to be scanned and determine the exposure settings for the fluorescent signals (up to 9) to be captured. The scanned field can be saved and reutilized when additional stains are employed to allow co-localization and registration with previous scanned images. Overall the functionality and quality of the images have been very suitable for histomorphometry and skeletal repair (see figure 10).

A major advantage of this instrument is a web based image sharing platform that allows investigator to view their images on their personal monitors as if they were look through the microscope. The can capture low power overviews or high power detail views selecting which color to emphasize or merge. Extensive planning was necessary with the company (Zeiss) and our institutional IT members to design the optimal structure for this capability. One computer local to the instrument will generate the image structure obtained from the instrument and send it

forward to a web server that will make it available to users. In addition, the files that the server will work from will be house in an institutional storage system that will also provide a backup capability. The hardware to implement these features has been purchased and currently is being installed. It will play a major role in coordinating the work in our 2010 ear mark proposal.

C. Implications for future research

As we have gained experience with the Mirax, image analysis, database design and user interaction, we are increasing drawn to the concept of centralized histology processing, imaging and database archiving as a national resource for skeletal research. We will be submitting proposal for the anticipated RFA for mouse phenotyping (skeletal tissue) that will be issued this fall as part of the mouse genome knock out project (proposal was submitted, but not funded). We believe that developing an atlas of GFP reporters and Cre-loxP drivers utilizing our approach would be of great values to the skeletal biology field. As mentioned above, a centralize system for evaluating skeletal repair strategies, not only would help to identify promising strategies, but could provide leadership to the FDA in developing the criteria for success in a preclinical model of skeletal repair.

Recently I had the opportunity to visit the development headquarters of Zeiss Microscope in Munich Germany to explain the concepts were are imaging for centralized digital imaging and image management. The instruments and software that they are developing will only further strength this concept. Just as centralized DNA sequencing and database management of sequencing information was crucial to the success of the human genome project, consistency in histology and imaging plus a structured basis for annotation, storage and retrival of visual biological information will be necessary for functional understanding of cells and genes important to skeletal repair. We want to be part of the team that builds this concept, and the opportunities provided by this DOD earmark project was the seed that has made us appreciate its importance and feasibility.

KEY RESEARCH ACCOMPLISHMENTS

A. Three models of bone repair (calvarial defect, closed fracture and long bone segmental defect) have been developed in GFP reporter mice that can be used to understand the cellular basis for a successful or failed tissue engineering protocol. The models have taught us that:

1. Donor derived bone formation is dependent on the quality of the progenitor cell that are implanted into the defect area. Whether mouse or human derived, continued passage and expansion rapidly destroys the progenitor activity.
2. Fresh bone marrow and non-adherant cells in a BMSC culture do not support intrinsic bone formation. The cells that line the surface of bone and are capable of systemic circulation are myeloid in origin and frequently express TRAP activity.
3. Progenitor derived from neonatal calvaria generate a membraneous like bone that show little trophism for interacting with host derived progenitor. In fact when implanted in a segmental defect, they appear to inhibit the periosteal response. In contract, progenitors derived from BMSC form a cortical like bone structure that is richly invested with bone marrow and which readily integrates with the surrouding bone. Thus all osteoprogenitors are not the same and the type of bone formed from any source of progenitor must be characterized.
4. The complexity of progenitors that develop in response to a closed fracture is very complex with at least three lineages, bone, cartilage and periosteum, arising from this population. The cells initiate their proliferation at the site that ultimately will be the base of the outer cortical shell, and they migrate centrally toward the fracture site. As they migrate they segregate into the three population of progenitors that will for periosteum, bone and cartialge. The function and control of each population needs to be understood to appreciate the factors necessary for a successful repair.

5. The segmental long bone defect also heals by periosteal expansion when sufficient progenitors cells fill the space above the defect to form an outer cortical shell. When the cells only fill the region between the to ends of the bone, then a pseudoarthrosis develops. Successful strategies for a segmental defect need to prevent the central intramedullary space to fill at the expense of filling the region extenal to the cortical bone, the region that will become the outer cortical shell.

B. The cryohistology, image analysis and database archiving of skeletal repair images provides a platform for improved experimentation of skeletal biology and repair:

1. The process for generating the histological sections is extremely rapid and more flexible than traditional paraffin or methyl methacyrlate histology.
2. Because all the fluorescent signals generated by the histology has biological meaning, image analysis can be performed by a computer using criteria that are observer independent and far more complex than can be done manually.
3. The image capture and analysis routines are readily applied to traditional static, dynamic and cellular histomorphometry of vertebra and femur, and the same concepts can be applied to the bone that is formed in a calvaria or segmental defect.
4. The digital images can be stored, annotated and retrieved in a database that allows multiple participants involved in a specific experiment to place their information in a single location. This avoids hunting through multiple hard drives to find data or the experimental condition that were used in an protocol.
5. We believe that the processing and imaging of skeletal repair data will provide a consistency of evaluation that cannot be achieved when histology is done at multiple sites. Depositing data centrally provides the opportunity to discover which protocol hold the great promise for success and could set the standard for the type of result needed for a preclinical model to be advance to larger animal or even human trials.

REPORTABLE OUTCOMES FOR YEAR 3-4

A. Publications:

1. Shin D-G., Hong, S-H., Joshi, P., Nori, R., Pei, B., Wang, H-W., Harrington, P., Kuo, L., Kalajzic, I., Rowe, D. (2009). "PBC: A Software Framework Facilitating Pattern-Based Clustering for Microarray Data Analysis", Proc. of ISIBM Int'l Joint Conf. on Bioinformatics., Sys. Bio. & Intell. Comp., pp. 31-36, Shanghai, China.
2. Shin, D-G., Kazmi, S., Baikang, P. Kim, Y-A., Maddox, J., Nori. R. Wong, A., Krueger, W., and Rowe, D. (2009). "Computing Consistencies between Microarray Data and Known Gene Regulation Relationships", IEEE Transactions on Information Technology in Biomedicine, 13(6):1075-82.
3. Ushiku, C., Jiang, X., Wang, L., Adams, D. and Rowe, D.W. in press. Long bone fracture repair in mice harboring GFP reporters for cells within the osteoblast lineage. J Orthop Res 28:1338-1347. PMID: 20839319.
4. Pei, B., Rowe, D.W., Shin, D-K. Learning Bayesian networks with integration of indirect prior knowledge. *Int. J. Data Mining and Bioinformatics,* 4:505-519. PMID: 21133038.
5. Kuhn LT, Liu Y, Advincula M, Wang YH, Maye P, Goldberg AJ., A Nondestructive Method for Evaluating In Vitro Osteoblast Differentiation on Biomaterials Using Osteoblast-Specific Fluorescence. Tissue Eng Part C Methods 16:1357-1366.
6. Yu, W., Xia, Z., Wang, L., Peng, F., Jiang, X, Huang, J., Rowe, D.W. and Wei, M. The Effect of Collagen/Apatite Scaffold Architecture on Bone Regenerative Properties. Manuscript for submission.
7. Ushiku, C., Adams, D.J., Jiang, X., Wang, L. and Rowe, D.W. Initial response of GFP-marked periosteal cells to bone fracture. Manuscript for submission.

8. Mori, Y., Jiang, X., Kalajzic, K., Maye, P., Shin, D-K, Adams, D., and Rowe, D.W. Dkk3-GFP reporter mice identify a progenitor cell population destined to form the fibrocartilage of the fracture callus. Manuscript for submission.
9. Hong, S-H., Jiang, X., Shin, D-G., and Rowe, D.W. Automated Fluorscence-based Dynamic and Cellular Bone Histomorphometry. Manuscript for submission.
10. Chaubey, A., Grawe, B., Dyment, N., Inzana, J., Jiang, X., Connolley, C., Goldstein, S.A., Awad, H., Rowe, D.W., Kenter, K., and Butler, D. Contrasting Structural and Biomechanical Responses of Sub-critical and Critical Defects on the Bone Healing Capacity in a Murine Femoral Non-Union Model. Manuscript for submission.
11. Wang, L., Jiang, X., Yu, X., Huang, J., Wei, M., Maye, P. and Rowe, D.W. Use of GFP Reporter Mice for Interpreting Cell-Based Models of Calvarial Defect Repair. Manuscript for submission.

B. Abstracts and Presentations:

1. Ushiku, C., Rowe, D.W., Jaing, X and Adams, D.J. Mice with Dual GFP Reporters of Osteoblast Lineage Elucidate Cellular Events in Fracture Healing. 56th Annual Meeting of the Orthopaedic Research Society, New Orleans, March 2009.
2. Ushiku, C., Rowe, D.W., Jaing, X and Adams, D.J. The Initial Response of GFP Reporter Periosteal Cells to Bone Fracture. 57th Annual Meeting of the Orthopaedic Research Society, Long Beach, Ca, Jan 2010.
3. Rowe, D.W., Wang, L, Jiang, X., Huang, J and Adams, D.J. Use of GFP Reporter Mice as an Evaluative Platform for Skeletal Repair. 2010 ATACCC, St. Petersburg, Fl., August, 2010
4. Rowe, D.W., Wang, L, Jiang, X., Huang, J., Ushiku, C and Adams, D.J. Use of GFP Reporter Mice as an Evaluative Platform for Skeletal Repair. Spotlight Session 57th Annual Meeting of the Orthopaedic Research Society. January 2010.
5. Wang, L., Jiang, X., Huang, J. and Rowe, D.W. Platform for Comparing In Vivo Bone Formation by Different Osteoprogenitor Cell Populations. MO0237. ASBMR 2010.
6. Rowe, D.W., Maye, P., Jiang, X, and Shin, D-G. Developing an Atlas of GFP Reporters and Cre Drivers of Interest to the Skeletal Biologist. FR0063. ASBMR 2010.
7. Hong, S-H., Jiang, X., Chen, L., Shin, D-G and Rowe, D.W. Fluorescence Based, Observer Independent Dynamic Bone Histomorphometry. SU0063. ASBMR 2010.
8. Rowe, D.W. Fluoresence-Based Dynamic and Cellular Histomorphometry of Murine Skeletal Structures Using Computer Controlled Imaging and Image Analysis. Meet the Professor session. ASBMR 2010
9. Maye, P., Fu, Y., Jiang, X., Liu, Y., Stover, M-L., Rowe, D.W. New Fluorescent Protein Reporter Animal Models to Study Skeletal Biology. SU0064. ASBMR 2010.
10. Xin, X., Stover, M-L., Liu, Y., Kuhn, L,n Rowe, D.W., Lichtler, A. Studies of Type I Collagen Mutations in Type I and IV Osteogenesis Imperfecta (OI) Patients Induced Pluripotent Stem (iPS) Cells. SA0151. ASBMR 2010.
11. Wang, L, Jiang, X., Huang, J., Chen, L. and Rowe, D.W. Murine Models for Evaluating Long Bone Segmental Repair. 2011 ATACCC, Fort Lauderdale, Fl., August, 2011.
12. Mori, Y., Jiang, X., Adams, D.J. and Rowe, D.W. A Dkk3 Reporter Identifies Progenitors of the Fibrocartilage and Periosteum of the Fracture Callus. ASBMR (platform presentation), 2011.
13. Wang, L., Jiang, X., Huang, J., Dyment, N., Chaubey, A. Butler, D., and Rowe, D.W. A Comparison of Murine Long Bone Segmental Defect Repair Models. ASBMR, 2011.

C. Training

1. Dr. Mori Yu began his two year postdoctoral fellowship with partial support from this award. The fellowship was terminated a year early due to the earthquake in his home town of Sendai, Japan.
2. Mr. Xiaohua Yu has completed his graduate student thesis on work performed and supported on this award.
4. Dr. Farhang Alaee, a orthopedic research fellow in Dr. Lieberman's laboratory was train in the cryohistology and imaging used in this project. He has had full access to the instrumentation required to generate the images and has work with Dr. Hong to develop image analysis routine for long bone skeletal defects.

D. Multidisciplinary interactions with tissue engineers and material scientists

1. A collaboration with Dr. Lakshmi Nair has lead to a funded grant of skeletal repair for which we will supply the surgical and histological platform.
2. Dr. Mei Wei's sabattical has developed into a long term collaboration with the longer time goal of real time 3D imaging of repair lesions using 2 photon imaging. Grant application to NIH on the topic was not funded.
3. Dr. Liisa Kuhn has shifted her effort to human progenitor cells and we have collaborated in evaluating the histological outcome of these experiments..
4. External relationships have developed with Dr. David Butler (Univ. Cincinnati), and Treena Arinzeh (New Jersey Institute of Technology).

D. Commercial Developments.

1. Two SBIR awards were continued to develop the image analysis process of mineralized tissue to dynamic histomorphometry and skeletal repair.
2. Obtained provisional patent protection of the histological, image analysis and database management for skeletal tissue will be filed. Effort to begin a commercial operation to provide these services to that broader research community are being developed.

CONCLUSION

The team that has work on this project are now well trained in their respective roles and are in a good position to optimize our approach for evaluating cellular and scaffold aspects of the bone formation aspect of skeletal repair. However the experience has been humbling for both the bone biologists and material scientists. *First*, the quality of the repair in regards to its integration into host bone and every for its long-term persistence has been called in to question by the work performed over the past year. We may have uncovered an unanticipated consequence of adding potent osteoprogenitor cells that may need detailed investigator to determine why the host bone does not participate in the repair process. Hopefully this problem can be overcome by the addition of various growth factors to the scaffold or the timing of introducing the donor progenitor cells relative to the prior activation of the host repair process. *Second*, the performance of scaffolds that were biocompatible in vitro did not prove to be osteogenic in vivo either due to technical issues related to detoxification or cell loading, or to the osteogenic properties of the scaffold material. These could not have been predicted and required a rapid and inexpensive method to work out these difficulties before more challenging repair models are attempted. In both cases, we should have the reagent mice and models to fully explore this critical determinant of a successful skeletal repair.

Long Bone Fracture Repair in Mice Harboring GFP Reporters for Cells within the Osteoblastic Lineage

Chikara Ushiku,[1] Douglas J. Adams,[1] Xi Jiang,[2] Liping Wang,[2] David W. Rowe[2]

[1]Department of Orthopedic Surgery, New England Musculoskeletal Institute, School of Medicine, University of Connecticut Health Center, Farmington, Connecticut 06032, [2]Center for Regenerative Medicine and Skeletal Development, Department of Reconstructive Sciences, Biomaterials and Skeletal Development, School of Dental Medicine, University of Connecticut Health Center, 263 Farmington Avenue, Farmington, Connecticut 06030

Received 10 September 2009; accepted 17 December 2009
Published online 29 March 2010 in wileyonlinelibrary.com. DOI 10.1002/jor.21105

ABSTRACT: GFP reporter mice previously developed to assess levels of osteoblast differentiation were employed in a tibial long bone fracture model using a histological method that preserves fluorescent signals in non-decalcified sections of bone. Two reporters, based on Col1A1 (Col3.6GFPcyan) and osteocalcin (OcGFPtpz) promoter fragments, were bred into the same mice to reflect an early and late stage of osteoblast differentiation. Three observations were apparent from this examination. First, the osteoprogenitor cells that arise from the flanking periosteum proliferate and progress to fill the fracture zone. These cells differentiate to osteoblasts, chondrocytes, to form the outer cortical shell. Second, the hypertrophic chondrocytes are dispersed and the cartilage matrix mineralized by the advancing Col3.6+ osteoblasts. The endochondral matrix is removed by the following osteoclasts. Third, a new cortical shell develops over the cartilage core and undergoes a remodeling process of bone formation on the inner surface and resorption on the outer surface. The original fractured cortex undergoes resorption as the outer cortical shell remodels inward to become the new diaphyseal bone. The fluorescent microscopy and GFP reporter mice used in this study provide a powerful tool for appreciating the molecular and cellular processes that control these fundamental steps in fracture repair, and may provide a basis for understanding fracture nonunion. J Orthop Res 28:1338–1347, 2010

Keywords: closed tibial fracture; GFP reporter mice; cryohistology of non-decalcified bone; osteoblast lineage; ELF97 substrate for osteoclasts

Long bone fracture is a time-tested model for evaluating the inherent ability of an experimental animal to activate the osteo/chondrogenic lineages for initial skeletal stabilization and subsequent coordination of the osteoblast/osteoclast lineages to remodel the immature callus back to a lamellar cortical bone.[1] The process can be altered by drugs [2–6] and genetic perturbations,[7–15] and is often used to examine the cellular/molecular basis of the perturbation on the osteogenic lineage.[16–18] The stages of fracture repair include the hemorrhagic/inflammatory exudate located in the proximity of the fracture zone,[19–21] an initial periosteal response at the margins of the fracture site,[22] the cartilaginous phase that forms the early structural stabilization across the fracture zone,[23] and development of the mineralized callus that will provide stiffness and strength as the cartilaginous zone is resorbed.[24,25] These complex modeling and remodeling activities must require a series of cellular events within the musculoskeletal lineage that control lineage fate decisions and modulate the extent of differentiation within each lineage. Furthermore, these fate and modulation decisions are not cell autonomous to the mesenchymal lineage. Vascular/endothelial cells that develop within the surrounding muscle must provide the oxygen tension essential for osteogenesis to progress[26,27] and potentially are a contributor to osteogenic progenitor cells.[28] The myeloid lineage not only provides the osteoclasts which are important to the remodeling cycle, but also macrophage and dendritic cells that are likely sources of cytokines.[19–21] Less well understood is the role of autonomic innervation to the remodeling process.[29,30]

In the process of developing GFP reporter mice that reflect levels of osteogenic differentiation, we have evolved a method for preserving GFP activity in non-decalcified bone that maintains the mineralization fluorochromes used to assess regions of new bone formation and allows for enzymatic stain of osteoclasts. By merging digital images obtained for individual fluorescent reporters and stains, it is possible to interrelate levels of osteoblast differentiation, regions of active mineralization, and sites of osteoclastic activity from the same section of mineralized tissue, and subsequently overlay the fluorogenic image with a chromogenic image.

This histological approach was applied to the tibial fracture model to determine if it can provide a greater appreciation of the dynamic and heterogeneous cellular aspects of fracture repair than traditional histology. A double transgenic reporter mouse was used throughout the study. The Col3.6GFPcyan (Col3.6 blue) reporter demonstrates low expression in preosteoblastic cells and becomes sharply stronger as matrix/mineral deposition capability is acquired. The human osteocalcin reporter, OcGFPtpz (Oc green), is associated with regions of strong mineralization in osteoblasts that are also Col3.6 blue positive.[31] The double positive cells show a spectrum of relative intensity, which may reflect the transition of an active matrix-forming osteoblast to a more metabolically quiescent bone lining cell. We will use a nomenclature that reflects the relative expression of each reporter in the double positive (DP) osteoblastic

Additional Supporting Information may be found in the online version of this article.
Figures 1–8 may be found at Wiley Interscience: http:www.interscience.wiley.com or for layered images at the author's website: http://rowelab.uchc.edu/RoweLabUCHC/

Correspondence to: David W. Rowe (T: 860-679-2324; F: 860-679-2910; E-mail: rowe@neuron.uchc.edu)

cells as Col3.6 blue>Oc green DP (toward active bone formation) and Oc green>Col3.6 blue DP (toward quiescent). For this study, the mice received a single dose of xylenol orange (XO) 1 day prior to sacrifice, which provides additional evidence for the mineralizing activity of overlying cells. Oc green only cells that are not associated with underlying mineralization are also observed on the surface of bone and may represent a bone lining cell. Osteoclasts were identified using a modified tartrate-resistant acid phosphatase (TRAP) stain and the fluorescent substrate ELF-97,[32] which emits a yellow wavelength signal that is distinct from the GFP signals. Presentation of the data follows the stages of fracture healing that have been developed previously, and the insights revealed by the new histology will be interpreted in the context of prior reviews of the topic.

METHODS

Mouse Breeding (See Supplement)

Male mice at 2–3 months of age were used in the study and were generated by crossing two GFP reporter mice, Col3.6GFPcyan and OcGFPtpz.[31] The institutional animal care committee approved all aspects of the experimental protocol. Details of the methods are in the supplemental data section.

Fracture Induction

A closed transverse diaphyseal fracture of the right tibia was performed under isoflurane anesthesia as described by Bonnarens and Einhorn.[1] Mice were sacrificed at day 1 to day 35 after fracture, with an intraperitoneal injection of xylenol orange (0.09 mg/kg) administered 1 day prior to sacrifice. The tibia was dissected free of the femur, ankle, and overlying skin, and sufficient muscle was retained to not disrupt the fracture zone. The sample was immersed in 4% buffered paraformaldehyde for 48 h in the cold with gentle rocking.

Processing and Staining the Samples (See Supplement)

The tibia was immersed in 30% sucrose dissolved in 0.1M PBS, pH 7.4 for 24 h. The tissue was positioned in Neg-50 Frozen Section Medium (Richard-Allan Scientific, Kalamazoo, MI), frozen on dry ice, and stored in air-tight plastic bags at −20°C until sectioning. Sagittal cryosections (5 μm) through the non-decalcified fracture callus were obtained on a Leica CM3050S cryostat (Leica, Wetzlar, Germany) using a disposable steel blade (Thermo, Fisher Scientific, Waltham, MA, MX35 PREMIER) and tape transfer process [Cryofilm Type2C (10), Section-lab, Hiroshima, Japan]. The tissue sections, which remain adherent to the tape through all of the subsequent steps, were placed sample side up on a glass slide and stored at −20°C until use.[33] After imaging the ELF-97 fluorochrome (Molecular Probes, Eugene, OR), the slides were rinsed in distilled water, stained in hematoxylin (Thermo, Shandon Instant Hematoxylin) for 2 min, and washed well in tap water.

Microscope Imaging

Sections were examined and photographed with a Zeiss Imager Z1 microscope (Carl Zeiss, Thornwood, NY) using Axio Vision Rel.4.7 (Carl Zeiss). The fluorescent signals were captured by a grayscale Zeiss Axiocam and pseudocolored to provide a visual contrast between the filters. XO was detected with a TRITC (red) filter (Chroma Technology, Bellows Falls, VT #31002), Col3.6cyan with a CFP (blue) filter (cat. #49001), and Octpz with a YFP (yellow–green) filter (cat. #49003). A differential interference contrast (DIC) image was acquired at the same time as the endogenous fluorescence imaging. Once completed, the slide was removed and stained with ELF97 and reimaged a second time with a yellow filter optimized for tetracycline (Chroma Technology Custom HQ409sp, 425dcxr, HQ555/30, set lot C-104285). The slide was removed again, stained with hematoxylin and imaged using a RGB chromogenic filter set (Zeiss, #487933) and reconstructed to provide a visual color image. The AxioVision software creates an image stack for each filter setting that is merged and exported as a flat file or exported as a multilayered jpg file for subsequent manipulation (e.g., Photoshop). The original higher resolution and more detailed images of each of the presented figures are available on a laboratory server (http://ucsci.uchc.edu/RoweLabUCHC/FigureX.tif where X=figure number). These images can be saved as tif files that can be viewed in Photoshop as layered images (under the window tab) that can be switched on and off to better appreciate and relate the expression of different color signals either within the same cells or to adjacent cells.

RESULTS

Activity of the GFP Reporters in Intact Bone

The growth plate of the 2–3-month-old mouse still has residual osteogenic activity and illustrates how the layered images are generated (see Supplemental Fig. 1 growth plate). The cut section is first imaged for endogenous fluorescent signals (GFP and XO) and under DIC to define the mineralized regions of the section (Supplemental Fig. 1B growth plate 2). Subsequently, the slide is removed from the stage and stained for TRAP activity in which the acidic conditions dissolve much of the mineral component of the tissue. The result is a section with yellow TRAP-positive cells of various size and the original osteogenic GFP, but removal of the red mineralization line (Supplemental Fig. 1 growth plate B-3). Once imaged, the slide is again processed for hematoxylin staining to provide visual orientation of the cellular elements with the corresponding GFP expression (Supplemental Fig. 1 growth plate B-1). The resulting merged image (Supplemental Fig. 1 growth plate B-4) shows hypertrophic chondrocytes and early mineralizing cartilage matrix which still contains remnants of dark-staining proteoglycan that are becoming surrounded by Col3.6 blue only or Col3.6 blue>Oc green DP cells with varying degrees of diffuse mineralization. Bright yellow osteoclastic cells line the bone surface and can be seen in the developing marrow space.

In contrast to the active growth plate, the cellular GFP pattern of the diaphysis shows regional zones of formation and resorptive activity (Fig. 1A, B). The endosteal surface near the proximal metaphysis shows a layer of Col3.6 blue>Oc green DP cells overlying a distinct red mineralization line, while on the opposing periosteal surface, there is a thin layer of yellow ELF97+ cells (Fig. 1C). However, in the central diaphysis, periosteal surfaces contain Oc green>Col3.6 blue DP and Oc green only cells that are not associated with mineralization (Fig. 1D). Thus, within the region where the fracture will be induced, the periosteum is

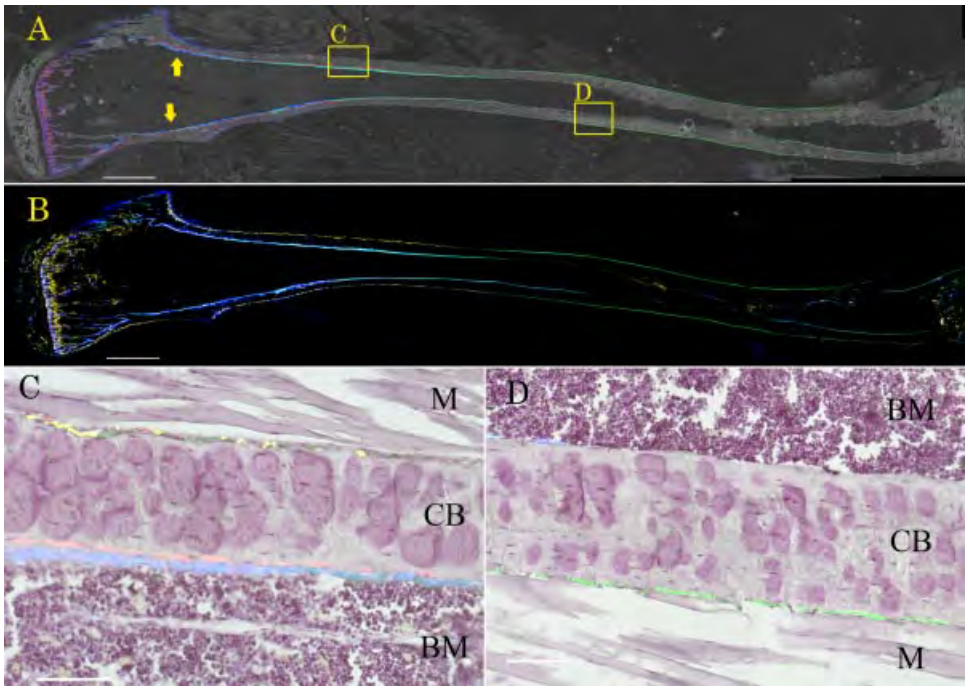

Figure 1. Activity of the GFP reporters in the intact unfractured tibial bone labeled with XO one day prior to sacrifice. A: Whole bone (5x, scale=1mm) scan that merges DIC, red (R), green (G) and blue (B) fluorescent filters. The endosteal surface shows continuing mineralization activity (red) and early osteogenic cells (blue) (arrows). Continued endosteal bone formation is evident in the metaphyseal region (region C) by Col3.6 blue>Oc green DP cells over a red label line. The diaphyseal bone shows no endosteal GFP activity but the periosteum is lined with Oc green>Col3.6 blue DP or Oc green only cells without the XO label. B: Repeat 5X bone scan after ELF97 staining now with the DIC removed. The yellow filter registers strong ELF97 activity in zone C and the linear arrangement of ELF97 cells in the periosteum of the metaphyseal region (region C) is revealed. Panels (C, D) are fully merged R,G,B,Y and RGB chromogenic images to align the fluorescent signals with the hematoxylin stain 20X views (scale = 100 μm of the corresponding 5X regions. In C, the periosteal bone near the metaphyseal region contains punctate areas of ELF97 positive cells interspersed with Oc green only cells without an XO label. The endosteal surface shows a mixture of Col3.6 blue>Oc green and Oc green>Col3.6 blue DP cells overlying the red XO mineralization line. In D the diaphyseal periosteal bone shows Oc green only cells and no GFP activity on the endosteal surface. M; Muscle CB; Cortical Bone BM; Bone Marrow. [Color figure can be viewed in the online issue, which is available at wileyonlinelibrary.com.]

composed primarily of quiescent bone lining osteoblasts and a low level of endosteal new bone formation.

Hemorrhagic/Inflammatory Stage

The collagen reporters that had been active in the diaphyseal region prior to fracture lose this activity in the periosteum flanking the fracture site 1–2 days after fracture (not shown). Blood and acute inflammatory cells accumulate within the central fracture zone and extend longitudinally beneath the periosteal membrane. The cells in this zone do not stain for ELF97 at this time.

Periosteal Proliferative Stage

The first change in osteogenic reporter activity begins on day 2 on the periosteal surface, well removed from the fracture zone (not shown). By day 4, a broad expansion of cells develops that is composed of three distinguishable cell types (Fig. 2). First and closest to the bone surface are the resident Oc green>Col3.6 blue DP cells that have changed their orientation from being parallel to oblique to the bone surface (Fig. 2B, yellow arrowhead). Some of the cells migrate away from the surface, appear to have increased in number, and are producing a matrix that has not yet begun to mineralize (star, Fig. 2D). Second, on top of and intermingled with the Oc green>Col3.6 blue DP cells are Col3.6 blue only cells (Fig. 2D). Third, above the Col3.6 blue only cells are a dense accumulation of myofibroblastic-shaped GFP-negative cells (Fig. 2B, arrow). These myofibroblastic cells appear to migrate into and fill the primary fracture zone, the region that eventually will be encapsulated by the outer cortical shell (Fig. 2C). Subsequent to the initial accumulation of the periosteal-derived myofibroblasts in the fracture zone, myofibroblastic cells that originate from surrounding muscle develop and appear to contribute to the total cellular population in the central fracture zone, but it is unclear if these later cells contribute to the developing callus. There is no ELF97 activity in the fracture zone at this time.

During this proliferative phase, the cells within the periosteum develop a gradient of cellular differentiation that progresses toward the fracture zone and, between days 4–6, completely fills the zone. At the leading edge are GFP-negative myofibroblastic cells that extend toward, and eventually fill, the central area that will become chondrocytes (Fig. 3B). Trailing the myofibroblastic cells is a triangular zone (see arrow in Fig. 3A) of GFP-positive cells in which the outer region contains Col3.6 blue only cells that initially are not associated with mineralization but do initiate

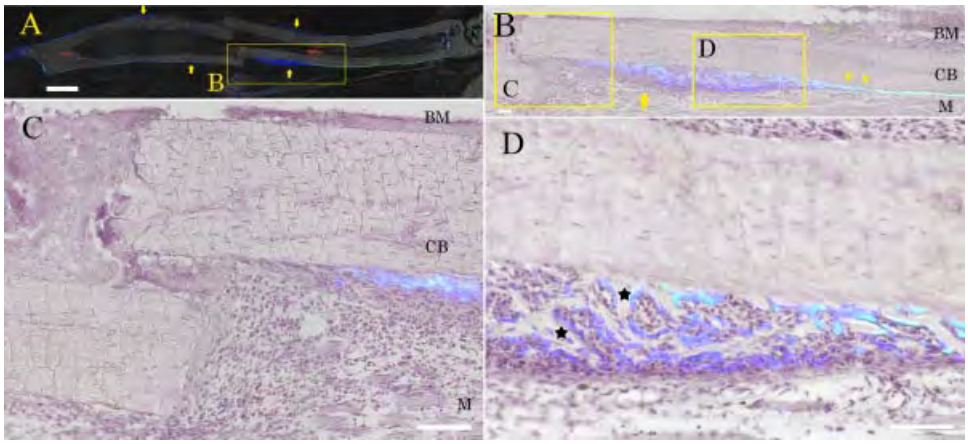

Figure 2. GFP expression at 4 days after fracture. Panel A. Bone scan at 5X with the G, R, B and DIC layers merged. The yellow arrows indicate the areas where the Col3.6 blue cells first appear. Panel B. 10X magnification of one of the proliferating periosteal regions that develops lateral to the fracture site. The R, G, B, Y and RGB images are merged. At this power a right to left transition from Oc green>Col3.6 blue DP (arrow head) to Col3.6 blue>Oc green DP to Col3.6 blue can be appreciated while the accumulation of GFP negative cells are present external to the GFP positive cells (arrow). The only ELF97 cells are present at this time are on the endosteal surface well removed from the fracture site. Panel C. 20X view closest to the fracture site shows the earliest activation of the bone lining cells (Col3.6 blue>Oc green DP without XO labeling) before the advancing wave of Col3.6 blue cells have developed. The entire fracture zone is now filled with GFP negative myofibroblastic cells. Panel D (20X) is the trailing zone in which the Col3.6 blue cells lie external to the oblique Col3.6 blue>Oc green DP bone lining cells both of which are associated with new matrix that has not yet begun to mineralize (stars). External to the Col3.6 blue cells is a more compact layer of GFP negative cells instead of the elongated myofibroblastic cells in the fracture zone. M; Muscle CB; Cortical Bone BM; Bone Marrow. [Color figure can be viewed in the online issue, which is available at wileyonlinelibrary.com.]

early mineralization 1–2 days later (Figs. 3A, B and 4A, B). At the periosteal base of the triangle are Oc green>Col3.6 blue cells that are in immediate contact with the cortical bone (star) and extend back to the bone lining cells (arrowhead in Fig. 3B).

The mineralization process in the triangular zone begins between days 5–7 as a diffuse red-granular deposit that surrounds and engulfs a small cluster of Col3.6 blue cells (Fig. 3C, green star; best appreciated by toggling on and off the red layer). Subsequently, the diffusely labeled cell cluster is surrounded by another layer of Col3.6 blue only or Col3.6 blue>Oc green DP cells that deposit a more linear mineralization band (Fig. 3C, green arrowheads, and Fig. 4D). The trailing region of the triangle contains intense Col3.6 blue>Oc green DP cells that show a distinct mineralization line and evidence of early bone marrow investment (Fig. 4D, star). Trailing behind the triangular zone are Oc green>Col3.6 blue DP cells that show a weaker mineralization line (Fig. 4B, yellow arrowhead).

During this phase, ELF97+ cells appear along the periosteal surface in the zone of early mineralization of Col3.6 blue>Oc green DP osteoblasts (Fig. 4C, arrows). They are absent from the zone of the most mature Oc

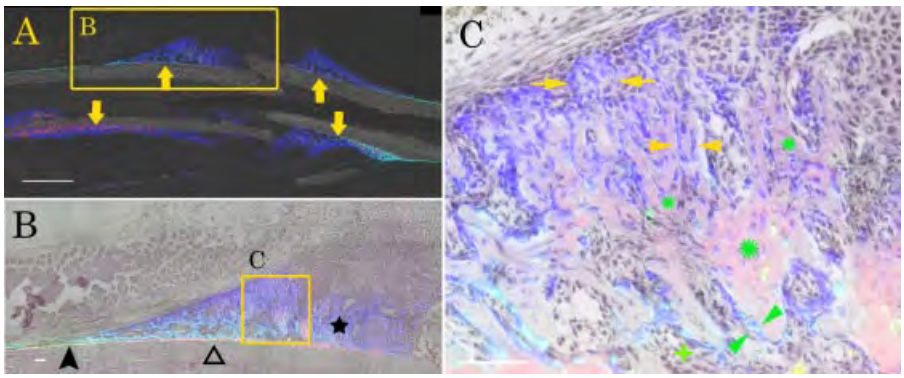

Figure 3. Fracture at day 6 demonstrating the beginning of mineralization in triangular zones and cartilage formation. Panel A (scale bar = 1mm) of the merged R,G,B and DIC images: 5x scan showing the triangular zones of early mineralized bone (yellow arrow in A) at the base cartilage callus. Panel B enlarges one of the triangular zones as it relates to other features of the fracture. The R, G, B, Y and RGB images are merged. The periosteal zone distal to the fracture site shows a transition of Oc green>Col3.6 blue DP cells (black arrow head in B) to Col3.6 blue>Oc green DP cells (open triangle in B) to Col3.6 blue only cells and little mineralization activity (black star in B). An area of the triangular zone is examined at 20X in panel C. The R, G, B, Y and RGB images are merged. Panel C shows the starting of mineralization in triangular zone are particularly in Col3.6 blue only populations. Diffuse red-granular deposit that surrounds and engulfs a small cluster of Col3.6 blue cells (green stared regions) which is better appreciated when the red layer is toggled off and on (see methods). This zone is bordered by another layer of Col3.6 blue only (yellow arrow heads) or Col3.6 blue>Oc green DP cells that deposit a more linear mineralization line (green arrow heads). Early marrow is developing in this zone (green cross). At the outer surface of the triangle the fibroblastic cells are mixed with Col3.6 blue only and do not mineralize (yellow arrows). [Color figure can be viewed in the online issue, which is available at wileyonlinelibrary.com.]

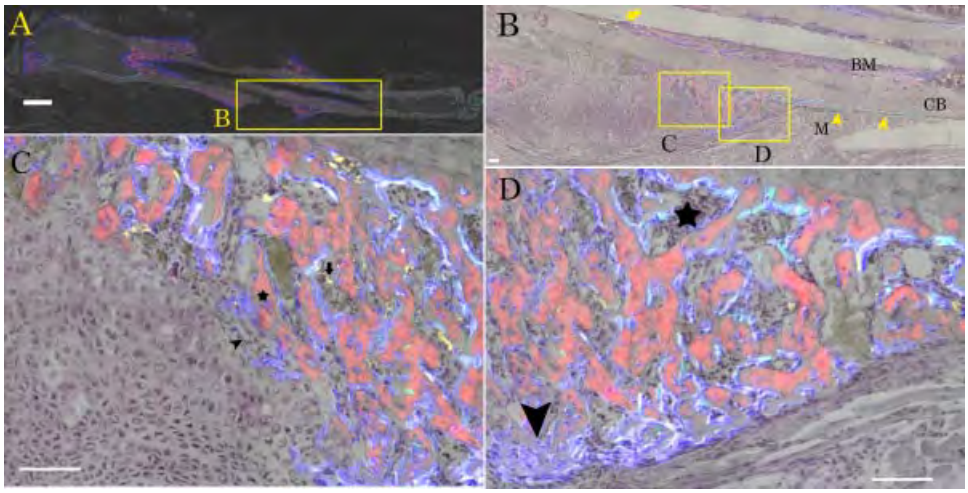

Figure 4. Fracture at day 7 demonstrating the transition from the proliferation to the cartilage removal stage of the repair. Panel A (scale bar = 1mm) of the merged R,G,B and DIC images: 5x scan showing the triangular zones of early mineralized (red) bone at the base of the cartilage callus. Panel B enlarges one of the triangular zones as it relates to other features of the fracture. The R, G, B, Y and RGB images are merged. The periosteal zone distal to the fracture site shows a transition of Oc green only to Oc green>Col3.6 blue DP cells and little mineralization activity (arrow head). Intense bone osteogenic activity is seen within the marrow space (BM) adjacent to the pin location with no evidence of directionality to suggest a process leading to fracture repair. One cluster of ELF97 cells has accumulated on the endosteal side at an apparent defect in the bone surface (arrow). Two areas (panels C and D) of the triangular zone are examined at 20X in which the R, G, B, Y and RGB images are merged. Panel C shows the junction between the cartilaginous and advancing bone cells just prior to the onset of cartilage matrix mineralization. From the cartilage cells, a 1-2 cell thick layer of GFP negative cells (arrow head) are followed by Col3.6 blue only cells that show early diffuse mineralization over the aggregation of blue only cells (star). It is adjacent to the clusters of diffusely XO mineralized cells that ELF97 positive cells first appear within the callus (arrow). Panel D is the more mature side of the triangle in which Col3.6 blue>Oc green DP cells develop on the surface of the matrix and begin to deposit a more distinct region of mineralization. Early marrow is developing in this zone (star) and the osteoclast density is much less than at the site of early osteoid mineralization. At the outer surface of the triangle, the cells remain deep blue and do not mineralize (arrow head). Beyond the Col3.6 blue cells are the densely packed elongated and GFP negative cell layer. These two cell populations will progress across the callus surface to eventually form the outer cortical shell. M; Muscle CB; Cortical Bone BM; Bone Marrow. [Color figure can be viewed in the online issue, which is available at wileyonlinelibrary.com.]

green>Col3.6 blue DP cells and have not yet appeared in the cartilage/bone interface. Varying degrees of endosteal bone formation are also observed, probably in response to the internal fixation pin, and this osteogenic activity does not extend into the fracture site (Fig. 4B). However, ELF97+ cells do accumulate on the endosteal surface near the fracture site and independent of coincident new bone formation (Fig. 4B, yellow arrow).

During the later stages of the proliferative stage, initial events that will produce the nascent cortical shell become evident. The outer surface of the triangle zone begins to extend outward along the distant surface of the central region (Fig. 4D, arrowhead), which by this time has achieved full chondrogenic differentiation (Fig. 4C). These cells are a lighter shade of Col3.6 blue only, do not make matrix, and are not mineralizing. External to the Col3.6 blue cells is a thin layer of dense elongated cells that do not express Col3.6 blue. During the subsequent cartilage removal stage, this process will continue to progress outward to meet its complement from the other side of the fracture (Fig. 5A).

Cartilage Removal Stage (Figs. 5 and 6)

Between days 7 and 14, the cells at the periphery of the cartilage become hypertrophic and generate a cartilage matrix with residual proteoglycan that stains a deep brown/red with hematoxylin, a feature which distinguishes it from the matrix made by Col3.6 blue cells (Fig. 5D). This matrix acquires a low degree of spontaneous mineralization prior to the in-growth of Col3.6 blue cells that forms a new mineralizing matrix over the cartilage matrix (Supplemental Fig. 5C-2, D-2). As the Col3.6 blue cells encroach on the cartilage core, most of the ELF97+ cells that enter the field first appear behind the Col3.6 blue/cartilage interface. This orientation suggests that the ELF97+ cells that invest the region primarily act on the mineralized tissue formed by Col3.6 blue cells and not on the cartilage matrix. By day 14, the entire region is filled with Col3.6 blue osteoblasts that overlie a mineralizing surface along with interspersed ELF97+ cells (Figs. 5B, and 6B, C). Oc green>Col3.6 blue DP cells remain at the periphery of the endochondral cartilage removal process (Figs. 5A and 6B).

As the nascent cortical shell develops during this time (Fig. 6), a thin layer of ELF97+ cells appear on the external surface of the structure (Fig. 6C, arrow). These ELF97+ cells are unusual because they are not associated with early mineralizing bone as occurs at other sites in the callus. ELF97+ clusters independent of Col3.6 blue cells also appear on the periosteal and endosteal surface of the original cortical bone (Fig. 6B, yellow arrowheads). In both areas, the ELF97+ cells create resorptive fields that will ultimately lead to dissolution of the original cortical bone and remodeling of the new cortical shell to replace the original cortical bone.

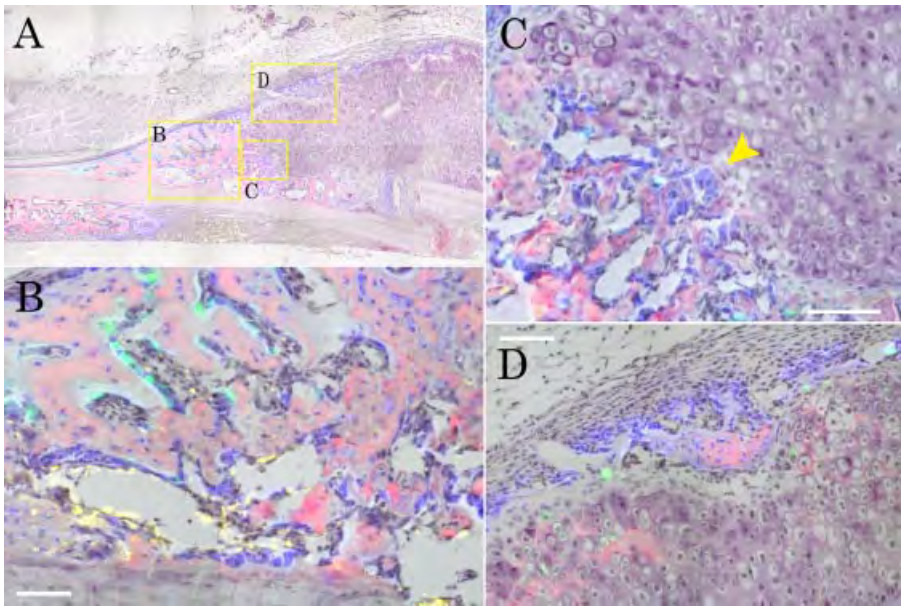

Figure 5. Day 10 after fracture illustrating the start of the cartilage resorption phase. Panel A: 5X (scale bar = 1mm) of the merged R,G,B and DIC images. Three areas of interest are shown at 10X. Panel B: Triangular zone and the interface of the osteoblast/chondrocyte junction. The R, G, B, Y and RGB images are merged and shows mineralizing Col3.6 blue>Oc green DP cells in regions in which the cartilage matrix has been replaced with osteoblast-derived matrix and an early marrow is being established. Panel C shows the interface between the Col3.6 blue and hypertrophic chondrocytes. The Col3.6 blue only cells tunnel between hypertrophic chondrocytes (arrow head) and deposit mineral on the residual cartilage matrix. As the mineralized matrix accumulates it becomes the template for the ELF97+ cells. The interface activity leads to immature bone formation along periosteal surface that is reaching the fracture site and is undermining the cartilage core. Pockets of osteoclastic activity along the endosteal and periosteal surface of the cortical bone develop at this time. Panel D shows the extension of the Col3.6 only cells along the outer surface of the callus that is capped by the elongated GFP negative cells. [Color figure can be viewed in the online issue, which is available at wileyonlinelibrary.com.]

Cortical Shell Formation and Remodeling Stage

Between days 14 and 21, the cortical shell develops intense matrix mineralization along the inner (neo-endosteal) surface and ELF97+ cells mediated bone resorption that is limited to the outer (neo-periosteal) surface (Fig. 7). The matrix-forming cells are strongly Col3.6 blue>Oc green DP and overlie a thick XO label. The cells contained within the base of the shell are more Oc green>Col3.6 blue DP with less mineralization (Fig. 7B, circle), while the cells at the base of the shell become Oc green only without a mineralization line (Fig. 7B, arrow). Underneath the shell, remnant areas of endochondral bone resorption continue. Both the new periosteal bone that extends onto the original cortical bone, as well as the original cortical bone, is sporadically lined with Oc green only cells without mineralization and clusters of ELF97+ cells (Fig. 8B, C, starred areas). Thus, these areas that were actively forming bone at an earlier time now show diminished activity and evidence of resorption. Late time points between 21 and 35 days show that the continued matrix-forming activity is limited to the endosteal surface of the callus shell that is associated with ELF97+ cells on the periosteal surface of the shell (Fig. 8). The Oc green only bone

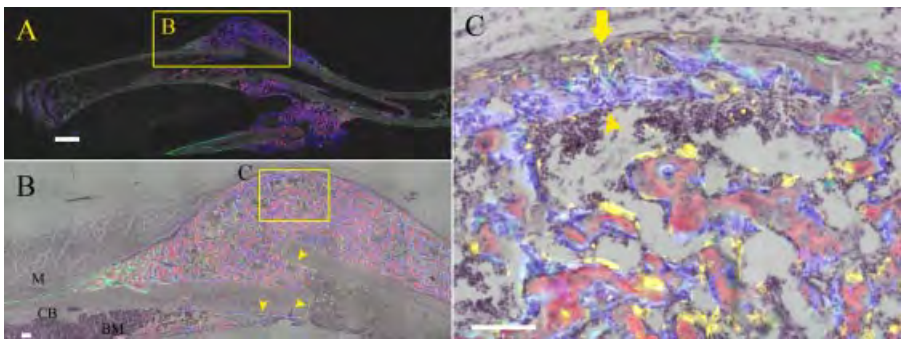

Figure 6. Day 14 demonstrating the cartilage resorption phase of fracture repair. Panel A is 5X scan merging the R,G,B and DIC images and showing diffuse mineralization of the cartilaginous zone. Panel B is a 10X merge of the R, G, B,Y and RGB filters to emphasize the distribution of ELF97 cells through out the cartilage region and surrounding the original cortical bone but not the mature Oc green>Col3.6 blue DP cells at the base of the callus. Panel C is a 20X image of the dome of the callus to illustrate the engulfed Col3.6 blue cells surrounding the residual cartilage matrix upon which are large (multinuclear) ELF97 positive cells. The R, G, B, Y and RGB images are merged. The organization of the nascent cortical shell is established as an outer dense GFP negative layer, followed by small ELF97 cells (arrow) and with Col3.6 blue cells (arrow head) on the inner surface that have not begun to deposit a mineralizing matrix. [Color figure can be viewed in the online issue, which is available at wileyonlinelibrary.com.]

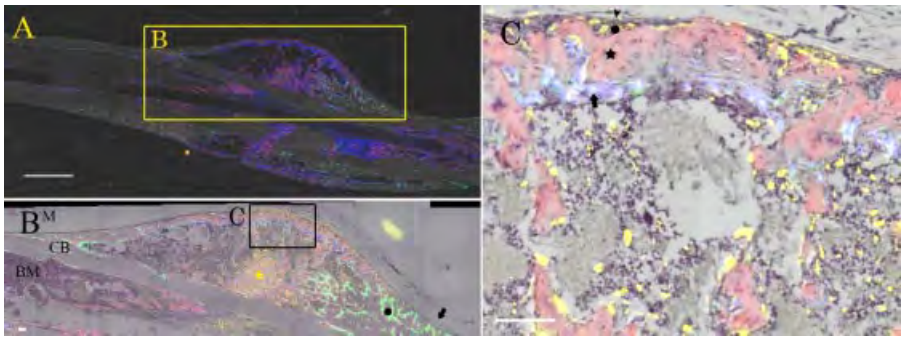

Figure 7. Day 21 of fracture demonstrating the transition from cartilage resorption to remodeling of the outer cortical shell phase of repair. Panel A is 5X showing an active outer cortical shell with residual resorbing mineralized cartilage near the fracture zone (asterix). Panel B is a 10X R,G,B, Y and RGB merged image of the cortical shell with the Col3.6 blue cells on the inner surface, underlying red mineralization line, followed by the yellow ELF97 osteoclasts and capped by the elongated GFP negative cells. In contrast, at the base of the callus are the Oc green>Col3.6 blue DP cells not associated with mineralization (arrow). Intense osteoclastic activity continues within the resorbing cartilaginous matrix (black star) as well as on the surface of the original cortical bone. Panel C is a 20X view of region C that details the layers of cells in the forming outer cortical shell. From out to inside the order is: GFP negative cells (arrow head) to small ELF97 cells (circle) to mineralized matrix (asterix) to Col3.6 blue>Oc green DP cells (arrow) and marrow lining cells. [Color figure can be viewed in the online issue, which is available at wileyonlinelibrary.com.]

lining cells that are characteristic of the quiescent diaphyseal periosteal zone show extension to the base of the new cortical shell but do not extend to the zone of active bone remodeling (Fig. 8B, C, arrowhead).

DISCUSSION

The advantage of GFP cryohistology within mineralizing tissue is the ability to associate dynamic tissue modeling and remodeling activity to a specific cell type or level of cellular differentiation within a heterogeneous cell population. It is also amenable to fluorescent-based in situ and immunostaining protocols which preserve the GFP signals and allows mapping these cellular activities to a specific cell population.[33,34] This work is designed to provide an organizational framework for future studies to understand cell transcriptional and signaling events at specific time points in fracture repair so that the tissue and genetic events that are required for a successful repair can be appreciated, and to identify critical steps that might lead to nonunion.

The long bone at the central diaphyseal site where the fracture was directed has quiescent bone lining cells on its periosteal surface with little or no endosteal osteogenic activity. In contrast, the cortical bone of the metaphyseal region has a low level of endosteal

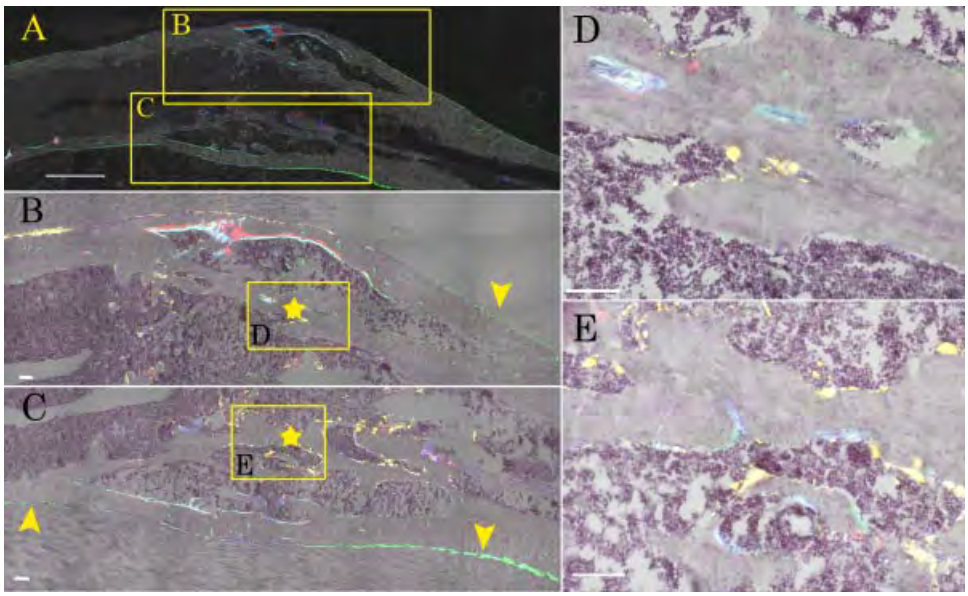

Figure 8. Day 35 post fracture showing the continuing remodeling of the outer cortical shell phase of repair. Panel A is a 5X view in which the outer cortical shell shows two states of remodeling. The upper shell (area B) is actively remodeling inward and panel B demonstrates the strong Col3.6 blue>Oc green DP cells overlying the red mineralization line and trailing osteoclast line. In Panel D, the Oc green>Col3.6 blue DP periosteal lining cells are present at the foot of the cortical shell. In the lower shell (area C) mineralizing Col3.6 blue>Oc green DP are present on the neo-endosteal side of the shell while Oc green>Col3.6 blue DP cells located on the periosteal side are extending toward the apex of the shell (arrow heads). Panels D and E are 20X view of the resorbing original cortical bone (outlined areas in panels B and C, respectively) that show numerous clusters of ELF97+ lining the bone surface. [Color figure can be viewed in the online issue, which is available at wileyonlinelibrary.com.]

remodeling. The Oc green only cells appear to mark a proportion of bone lining cells, but it is likely that additional lining cells are present that do not express the GFP reporter. With induction of the fracture, GFP activity adjacent to the fracture zone disappears. In this model, the early hemorrhagic and acute inflammatory exudate remains in the immediate vicinity of the fracture area and extends into the periosteum. Presumably, it is the release of factors from within the clot area or the nerve-rich periosteum, and perhaps an alteration in mechanical forces across the uninjured cortical bone, that are responsible for the periosteal response that will begin the healing process.

The first periosteal response to the fracture is seen in the bone lining cells that flank the fracture site and that maintained their GFP expression. During the first 1–2 days postfracture, there is an expansion of the Oc green>Col3.6 blue DP lining cells above the bone surface and the appearance of overlying and admixed GFP-negative myofibroblastic cells, some of which differentiate to Col3.6 blue only cells. By day 4, this myofibroblastic/Col3.6 blue only population advances toward the fracture area as a triangular zone of cells. These cells represent different levels of cellular proliferation, migration, and differentiation within the osteogenic lineage. What is unclear from our examination is whether they arise by dedifferentiation of lining cells, expansion of resident early progenitors, recruitment of vascular pericytes within the periosteal membrane, or a combination of all possibilities.

Between days 4 and 7, the leading edge of the triangular region advances and expands to fill the fracture zone. These cells are highly motile multipotential progenitors that precede the onset of Col3.6GFP expression. The cells that reach the central zone differentiate to chondrocytes, while cells that trail behind or migrate to the outer zone of the callus will eventually become osteoblasts. What determines the differentiation choice is not known, although the ambient oxygen tension of the region is likely to have a major influence. Often the cartilage zone is partially separated by a wedge of fibroblastic cells that appear to have originated from the surrounding muscle. Critical experiments to determine if the muscle-derived myofibroblastic cells contribute to bone or cartilage need to be performed to assess the direct or indirect role of the surrounding skeletal muscle to formation of the initial callus. The extent that the fracture zone is populated with these multipotential progenitor cells is likely to be a most critical factor in determining the course of fracture repair.[3,7,10,23]

The trailing region of the triangular area shows a gradient of increasing osteoblast differentiation. Col3.6 blue only cells begin the mineralization process and, as matrix accumulates, these osteoblasts (Col3.6 blue cells) become Col3.6 blue>Oc green DP and ELF97+ cells appear. Beyond the ELF97+ region, less mineralization is evident and the osteoblasts have become Oc green>Col3.6 blue DP. The Oc green>Col3.6 blue DP cells closest to the original bone surface are the first to deposit a mineralizing matrix, but as the triangle zone progresses, this initial site of bone formation changes to become Oc green>Col3.6 blue DP without mineralization. The ability of the early lineage osteoblast to progress to full osteoblast differentiation in an ordered manner is likely to be another critical requirement for efficient fracture repair.

From 7 to 21 days, the chondrocytes and cartilage matrix are completely removed.[35] The steps of removal follow a spatial sequence of Col3.6 blue osteoblasts depositing a mineralizing matrix on the cartilage template, followed by the appearance of ELF97+ cells in close proximity with the Col3.6 blue cells. This sequence of cellular advance is consistent with the observation that MMP13 is produced by cells in the osteogenic lineage,[36] and mice deficient in MMP13 function have a defect in cartilage removal that cannot be rescued with normal bone marrow.[14,37] However, the ELF97+ osteoclasts that follow the Col3.6 cells synthesize MMP9,[38] and mice deficient in this collagenase also have a cartilage removal defect.[39] Once the early osteoblast in-growth phase is completed, the entire cartilagenous zone is filled with osteoclasts and the intensity of the Col3.6 blue activity diminishes. The advancement of the Col3.6 blue cells presumably is dependent on the MMP13 that are highly expressed in early osteoblastic cells,[40] while the removal phase of the mineralized cartilage is dependent on the activity of the osteoclasts. The removal is critical for the final resolution of the fracture, as studies using agents that block osteoclast activity have a persistent unresorbed mineralized callus.[5,6,41]

As the cartilage removal process progresses, the outer layer of the callus establishes the structure that will form a new cortical shell.[42–44] The Col3.6 blue cells populate the inner (neo-endosteal) surface of the shell, which is followed by a thin layer of ELF97+ cells and a layer of GFP-negative myofibroblastic cells on the outer (periosteal) surface. By 21 days, the outer cortical shell is fully formed and has a distinctive dynamic form. A layer of Col3.6 blue>Oc green DP cells line the endosteal surface and overlays an unusually thick mineralization line. On the periosteal side of the recently formed bone matrix is a layer of ELF97+ cells. Initially, the entire endosteal surface of the cortical shell is active, but as the base of the shell thickens, the active formation area contracts outward toward the apex of the shell. The process of remodeling inward from the convex cortical shell resembles the process observed in the metaphyseal region of normal cortical bone. As the cortical shell remodels inward, the original cortical bone and accumulated new bone on its surface appears to be undergoing a gradual resorption process. The bone contains osteoblasts that are primarily Oc green only without associated mineralization and numerous clusters of osteoclasts on the bone surface. At this stage of repair, judicious loading of the fracture zone would likely affect remodeling of

the cortical shell as it replaces the original cortical bone.[45,46]

The recent publications by McDonald et al.[5] and Gerstenfeld et al.[6] that examine the effect of bisphosphonates and Rank ligand binding monoclonal antibodies on fracture repair can be interpreted in the light of the fluorescent-based histology to better appreciate the interdependent roles of the osteoblast and osteoclast lineages in fracture stabilization and resolution. Bone formation, as it occurs at the base of the callus and extends over the surface of the callus to form the periosteum and outer cortical shell, is driven primarily by the differentiation of osteoblasts from the periosteal progenitors. Similarly, the chondrocytes within the central fracture zone are a product of this progenitor population. The osteoclast inhibitors do not affect these early steps in fracture repair. However, the subsequent remodeling of these structures requires the osteoclast, as evidenced by the delay of inward remodeling of the formed outer cortical shell and the failure to resorb the mineralized cartilage core.

The inward remodeling of the cortical shell is associated with active osteoclasts on the periosteal surface of the shell, as well as osteoblastic activity on the endosteal surface. An increased bone volume is one measure of this lack of remodeling, as observed in the osteoclast-inhibited rodent studies. It would be predicted that the inhibition of the osteoclastic activity would also increase the thickness of the shell. More revealing is the consequence of osteoclast inhibition to resolution of the cartilage core. The fact that the cartilage becomes mineralized suggests that the invasion of the immature osteoblasts into the hypertrophic cells was not impaired, and an immature osteoid was produced that supported intense mineralization. However, the subsequent step of osteoclast attraction to, and resorption of, the osteoblast-produced matrix that overlies the cartilage matrix did not occur. The result is a large unresorbed mineralized composite structure (thickened cortical shell and trabecular struts, and mineralized woven bone/cartilage matrix amalgam), that in bulk provided greater strength to the fracture region despite poor material properties, than the bony structure that forms the remodeling outer cortical shell.

Two other observations in the resolving fracture point to the importance of osteoclast function independent of mechanical properties. First is the apparent paucity of bone marrow formation within the remodeling callus in the osteoclast-inhibited mice, as noted in the paper of Gerstenfeld and coworkers.[6] The appearance of osteoclasts is strongly associate with the accumulation of bone marrow elements and the maturation of the Col3.6blue to Oc-green>Col3.6blue cells that we associate with formation of a less woven and more highly mineralized bone structure. This change in osteoblast maturity is first observed at the base of the callus and extends upward toward the outer cortical shell. Trabecular elements that form internal to the outer cortical shell also demonstrate this transition, although in most cases these structures appear to be either resorbed or incorporated into the inwardly remodeling cortical shell. Second is the resorption of the original cortical bone that is internal to the outer cortical shell. These structures attract osteoclasts in the absence of osteoblastic activity, and increasingly acquire a moth-eaten structure. Inhibition of osteoclast activity would be expected to block this resorption process, and persistence of the original cortical bone was observed in these two rodent studies.

Our study suggests that three critical phases to fracture repair can be identified: multipotential periosteal progenitor proliferation, migration, and differentiation; cartilage removal; and cortical shell bone remodeling (see Supplemental Figs. 2 and 3). Each phase has a complex cellular and molecular basis that will require separate experimental approaches to fully understand. GFP reporters for all of the potential cellular participants now exist and can be combined with some of the reporters used in the present study to provide context to the ongoing repair process. Associating fluorescent immunostaining or in situ studies with a cell-specific GFP reporter will provide additional molecular and signaling detail to identify targets or processes that are critical to the repair process.

ACKNOWLEDGMENTS

This work was funded by The U.S. Army Medical Research and Materiel Command, contract W81XWH-07-2-0085, and grants R01-AR043457 and R01-AR052374 from the National Institutes of Health, to D. W. R.

REFERENCES

1. Bonnarens F, Einhorn TA. 1984. Production of a standard closed fracture in laboratory animal bone. J Orthop Res 2:97–101.
2. Li J, Mori S, Kaji Y, et al. 2000. Concentration of bisphosphonate (incadronate) in callus area and its effects on fracture healing in rats. J Bone Miner Res 15:2042–2051.
3. Nakazawa T, Nakajima A, Shiomi K, et al. 2005. Effects of low-dose, intermittent treatment with recombinant human parathyroid hormone (1-34) on chondrogenesis in a model of experimental fracture healing. Bone 37:711–719.
4. Kaback LA, Soung do Y, Naik A, et al. 2008. Teriparatide (1-34 human PTH) regulation of osterix during fracture repair. J Cell Biochem 105:219–226.
5. McDonald MM, Dulai S, Godfrey C, et al. 2008. Bolus or weekly zoledronic acid administration does not delay endochondral fracture repair but weekly dosing enhances delays in hard callus remodeling. Bone 43:653–662.
6. Gerstenfeld LC, Sacks DJ, Pelis M, et al. 2009. Comparison of effects of the bisphosphonate alendronate versus the RANKL inhibitor denosumab on murine fracture healing. J Bone Miner Res 24:196–208.
7. Taylor DK, Meganck JA, Terkhorn S, et al. 2009. Thrombospondin-2 influences the proportion of cartilage and bone during fracture healing. J Bone Miner Res 24:1043–1054.
8. Gaur T, Wixted JJ, Hussain S, et al. 2009. Secreted frizzled related protein 1 is a target to improve fracture healing. J Cell Physiol 220:174–181.
9. Kellum E, Starr H, Arounleut P, et al. 2009. Myostatin (GDF-8) deficiency increases fracture callus size, Sox-5 expression, and callus bone volume. Bone 44:17–23.

10. Yamakawa K, Kamekura S, Kawamura N, et al. 2008. Association of microsomal prostaglandin E synthase 1 deficiency with impaired fracture healing, but not with bone loss or osteoarthritis, in mouse models of skeletal disorders. Arthritis Rheum 58:172–183.
11. Schindeler A, Morse A, Harry L, et al. 2008. Models of tibial fracture healing in normal and Nf1-deficient mice. J Orthop Res 26:1053–1060.
12. Rundle CH, Wang X, Sheng MH, et al. 2008. Bax deficiency in mice increases cartilage production during fracture repair through a mechanism involving increased chondrocyte proliferation without changes in apoptosis. Bone 43:880–888.
13. Rundle CH, Wang X, Wergedal JE, et al. 2008. Fracture healing in mice deficient in plasminogen activator inhibitor-1. Calcif Tissue Int 83:276–284.
14. Kosaki N, Takaishi H, Kamekura S, et al. 2007. Impaired bone fracture healing in matrix metalloproteinase-13 deficient mice. Biochem Biophys Res Commun 354:846–851.
15. Li M, Healy DR, Li Y, et al. 2005. Osteopenia and impaired fracture healing in aged EP4 receptor knockout mice. Bone 37:46–54.
16. Tsuji K, Bandyopadhyay A, Harfe BD, et al. 2006. BMP2 activity, although dispensable for bone formation, is required for the initiation of fracture healing. Nat Genet 38:1424–1429.
17. Yukata K, Matsui Y, Shukunami C, et al. 2008. Altered fracture callus formation in chondromodulin-I deficient mice. Bone 43:1047–1056.
18. Tsuji K, Cox K, Bandyopadhyay A, et al. 2008. BMP4 is dispensable for skeletogenesis and fracture-healing in the limb. J Bone Joint Surg [Am] 90(Suppl 1) 14–18.
19. Takamiya M, Fujita S, Saigusa K, et al. 2008. A study on mRNA expressions of interleukin 10 during fracture healing for wound age determination. Leg Med (Tokyo) 10:131–137.
20. Lehmann W, Edgar CM, Wang K, et al. 2005. Tumor necrosis factor alpha (TNF-alpha) coordinately regulates the expression of specific matrix metalloproteinases (MMPS) and angiogenic factors during fracture healing. Bone 36:300–310.
21. Gerstenfeld LC, Cho TJ, Kon T, et al. 2003. Impaired fracture healing in the absence of TNF-alpha signaling: the role of TNF-alpha in endochondral cartilage resorption. J Bone Miner Res 18:1584–1592.
22. Nakajima A, Nakajima F, Shimizu S, et al. 2001. Spatial and temporal gene expression for fibroblast growth factor type I receptor (FGFR1) during fracture healing in the rat. Bone 29:458–466.
23. Nakajima F, Ogasawara A, Goto K, et al. 2001. Spatial and temporal gene expression in chondrogenesis during fracture healing and the effects of basic fibroblast growth factor. J Orthop Res 19:935–944.
24. Nakajima A, Shimoji N, Shiomi K, et al. 2002. Mechanisms for the enhancement of fracture healing in rats treated with intermittent low-dose human parathyroid hormone (1-34). J Bone Miner Res 17:2038–2047.
25. Gerstenfeld LC, Alkhiary YM, Krall EA, et al. 2006. Three-dimensional reconstruction of fracture callus morphogenesis. J Histochem Cytochem 54:1215–1228.
26. Deckers MM, van Bezooijen RL, van der Horst G, et al. 2002. Bone morphogenetic proteins stimulate angiogenesis through osteoblast-derived vascular endothelial growth factor A. Endocrinology 143:1545–1553.
27. Zelzer E, Glotzer DJ, Hartmann C, et al. 2001. Tissue specific regulation of VEGF expression during bone development requires Cbfa1/Runx2. Mech Dev 106:97–106.
28. Kalajzic Z, Li H, Wang LP, et al. 2008. Use of an alpha-smooth muscle actin GFP reporter to identify an osteoprogenitor population. Bone 43:501–510.
29. Graham S, Hammond-Jones D, Gamie Z, et al. 2008. The effect of beta-blockers on bone metabolism as potential drugs under investigation for osteoporosis and fracture healing. Expert Opin Invest Drugs 17:1281–1299.
30. Huang HH, Brennan TC, Muir MM, et al. 2009. Functional alpha1- and beta2-adrenergic receptors in human osteoblasts. J Cell Physiol 220:267–275.
31. Bilic-Curcic I, Kronenberg M, Jiang X, et al. 2005. Visualizing levels of osteoblast differentiation by a two-color promoter-GFP strategy: type I collagen-GFPcyan and osteocalcin-GFPtpz. Genesis 43:87–98.
32. Filgueira L. 2004. Fluorescence-based staining for tartrate-resistant acidic phosphatase (TRAP) in osteoclasts combined with other fluorescent dyes and protocols. J Histochem Cytochem 52:411–414.
33. Jiang X, Kalajzic Z, Maye P, et al. 2005. Histological analysis of GFP expression in murine bone. J Histochem Cytochem 53:593–602.
34. Salie R, Li H, Jiang X, et al. 2008. A rapid, nonradioactive in situ hybridization technique for use on cryosectioned adult mouse bone. Calcif Tissue Int 83:212–221.
35. Lee FY, Choi YW, Behrens FF, et al. 1998. Programmed removal of chondrocytes during endochondral fracture healing. J Orthop Res 16:144–150.
36. Nakamura H, Sato G, Hirata A, et al. 2004. Immunolocalization of matrix metalloproteinase-13 on bone surface under osteoclasts in rat tibia. Bone 34:48–56.
37. Behonick DJ, Xing Z, Lieu S, et al. 2007. Role of matrix metalloproteinase 13 in both endochondral and intramembranous ossification during skeletal regeneration. PLoS One 2:e1150.
38. Andersen TL, del Carmen Ovejero M, Kirkegaard T, et al. 2004. A scrutiny of matrix metalloproteinases in osteoclasts: evidence for heterogeneity and for the presence of MMPs synthesized by other cells. Bone 35:1107–1119.
39. Colnot C, Thompson Z, Miclau T, et al. 2003. Altered fracture repair in the absence of MMP9. Development 130:4123–4133.
40. Itagaki T, Honma T, Takahashi I, et al. 2008. Quantitative analysis and localization of mRNA transcripts of type I collagen, osteocalcin, MMP 2, MMP 8, and MMP 13 during bone healing in a rat calvarial experimental defect model. Anat Rec (Hoboken) 291:1038–1046.
41. Amanat N, McDonald M, Godfrey C, et al. 2007. Optimal timing of a single dose of zoledronic acid to increase strength in rat fracture repair. J Bone Miner Res 22:867–876.
42. Li J, Mori S, Kaji Y, et al. 1999. Effect of bisphosphonate (incadronate) on fracture healing of long bones in rats. J Bone Miner Res 14:969–979.
43. Cao Y, Mori S, Mashiba T, et al. 2002. Raloxifene, estrogen, and alendronate affect the processes of fracture repair differently in ovariectomized rats. J Bone Miner Res 17: 2237–2246.
44. Komatsubara S, Mori S, Mashiba T, et al. 2005. Human parathyroid hormone (1-34) accelerates the fracture healing process of woven to lamellar bone replacement and new cortical shell formation in rat femora. Bone 36:678–687.
45. Goodship AE, Lawes TJ, Rubin CT. 2009. Low-magnitude high-frequency mechanical signals accelerate and augment endochondral bone repair: preliminary evidence of efficacy. J Orthop Res 27:922–930.
46. Isaksson H, Grongroft I, Wilson W, et al. 2009. Remodeling of fracture callus in mice is consistent with mechanical loading and bone remodeling theory. J Orthop Res 27:664–672.